Geometry Determination of Biogas Storage Systems

Master Thesis

By

Lukas Sint, BSc

Graz University of Technology
Engineering Geodesy and Measurement Systems

Supervisor:
Univ. Prof. Dr. Werner Lienhart

Graz, Mai 2014

In cooperation with:
Sattler AG:

Division Membrane Solutions
Environment Engineering

Acknowledgements

Statutory Declaration

I declare that I have authored this thesis independently, that I have not used other than the declared sources / resources, and that I have explicitly marked all material which has been quoted either literally or by content from the used sources.

…………………………   …………………………………………..
          Date   (signature)

Abstract

Biogas is a promising renewable energy source, which is being produced all across Europe. For efficient energy production, biogas storage systems are needed, whereas biogas storage systems made from textile membranes are most promising, since they are easy to install, inexpensive and the membranes do not react with H_2S (Hydrogen Sulfide), a corrosive side product of the digestion. Such double membrane storage systems have an outer membrane, either filled with air to support it or held by a mast, and an inner membrane which holds the biogas. Spherical shapes are commonly used, since the pressure is ideally distributed along all welding seams. This shape is built by welding of different plane cutouts, which leads to deformations at the welding seams and the pole area. These differences to the ideal shape put more stress on certain parts of welding seams and have an effect on the durability of the whole storage system. To further improve the manufacturing process, 3D measurements of the real geometry are needed. This thesis gives an review on different measurement systems used in industrial surveying and geodesy. After exploring different approaches towards 3D measurement systems, a ¾ test sphere is measured and compared to a reference model. The resulting point cloud shows the differences to the reference model and can be used for further investigations.

Kurzfassung

Biogas wird heute als erneuerbarer und nachhaltiger Energieträger verstanden, der mittlerweile an einer großen Anzahl von Standorten in ganz Europa produziert wird. Für eine effiziente Energieproduktion sind Biogasspeicheranlagen notwendig, wobei von den verschiedenen Bauarten Biogasspeicher mit Doppelmembran größtes Zukunftspotential aufweisen. Dies kommt daher, dass solche Biogasspeicher kostengünstig und einfach zu installieren sind und die speziell beschichtete Membran nicht mit H_2S (Schwefelwasserstoff), einem korrosiven, giftigen Nebenprodukt der Vergärung von organischen Stoffen reagiert. Solche Biogasspeicher besitzen jeweils eine Außenmembran, welche entweder durch Luftdruck die Form behält oder von einem Stützmast gehalten wird und eine Innenmembran, welche das Biogas speichert. Eine häufige Form solcher Speicher ist die ¾ Kugel. Diese wird aus ebenen Zuschnitten gefertigt, was zur Folge hat, dass die Kugelform nicht perfekt zu realisieren ist und es dadurch u. a. zu Krümmungsänderungen an den Schweißnähten kommt. Dadurch entstehen höhere Spannungen an den Schweißnähten, was wiederum die Lebensdauer der Biogasspeicheranlage beeinflussen kann. Um nun den Produktionsprozess zu verbessern, sind 3D Messwerte der realen Geometrie nötig. In dieser Arbeit werden verschiedene Ansätze für die 3D Erfassung von Objekten aus der Industrievermessung und dem Vermessungswesen beschrieben. Um die gesamte Kette von Aufnahme bis Interpretation durchzuführen, wurde ein ¾ Test Speicher mit einem geeigneten Messsystem aufgenommen und mit einem Referenzmodell verglichen. Als Ergebnis erhält man so eine Punktwolke mit Informationen zu Abweichungen vom Referenzmodell.

Preamble

The company Sattler AG approached Graz University of Technology with the question "How does the real geometry of biogas storage systems look in detail?" The three main aspects of this question are

1) How does the real geometry of the outer membrane differ from the reference model, calculated from a finite element model?
2) How does the membrane behave around the welding seams in contrast to constant curvature?
3) How does the inner membrane behave with different filling levels?

The Institute for Engineering Geodesy and Measurement Systems (EGMS) of Graz University of Technology was asked to give an overview and recommendation of different 3D measurement systems and to resolve the first aspect. The cooperation between Sattler AG and the Graz University of Technology should then continue for the aspects 2 and 3.

Table of Contents

List of Figures

List of Tables

1 Introduction

1.1 Biogas Technology

Today's world depends on fossil fuels like petroleum and coal, which become more and more scarce and also have a negative impact on global climate. This leads to research in different fields to get access to new sources of energy. Especially renewable energies, like solar, wind, different kinds of thermal and hydro energy and biogas, are the most promising energy sources to counter the aforementioned problems. Biogas technology in particular offers unique opportunities. Biogas can be produced from organic waste, grown resources like energy plants, waste products of industrial food production and sewage sludge, while at the same time producing fertilizer for agricultural uses. There is no geographical limitation, since the anaerobic digestion is a controlled biological degradation process which allows efficient capturing and utilization of biogas for energy generation (Salunkhe, 2012). Figure 1 shows a schematic representation of such a biogas plant, where the produced biogas is used in a combined heat and power generation plant. Substrate, for example liquid manure, is introduced to the digester. Here the anaerobic digestion sets in, while an agitator stirs the substrate. This produces biogas, which comprises primarily of methane (CH_4), carbon dioxide (CO_2) and small amounts of hydrogen sulfide (H_2S). With cogeneration, also known as combined heat and power (CHP), the production of electricity and heat from the biogas can be achieved. A portion of the heat can be used as fermentation heat in the digester. Leftover substrate can still be used as fertilizer.
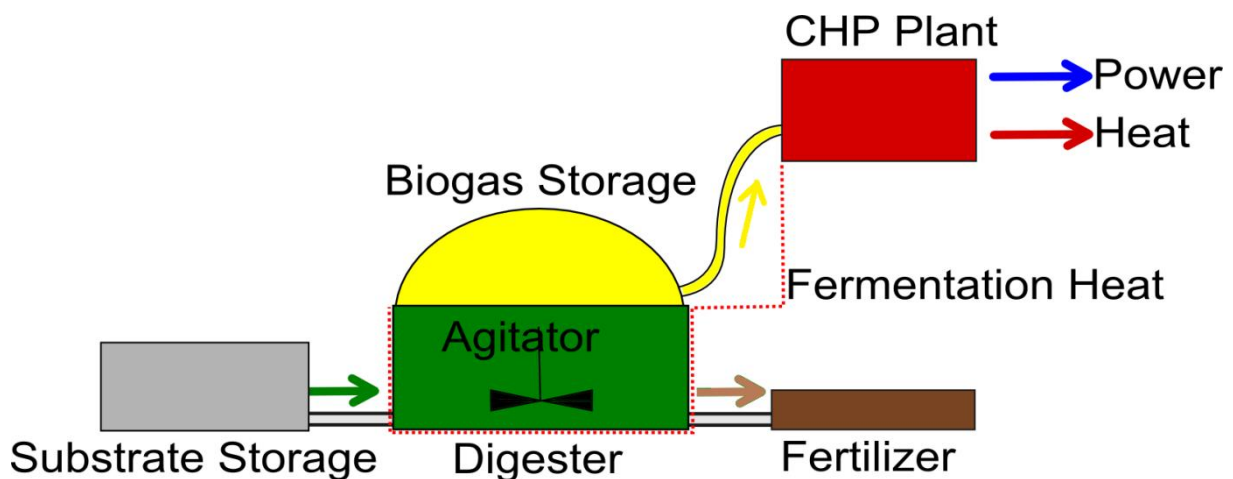
Figure 1: Schematic representation of a biogas plant

In 2008 there were 340 registered biogas plants in Austria. The production of biogas per hour per plant was 40m³ to 400m³, which covers about 1% of the Austrian energy requirements (Tragner, 2008). In Germany over 7500 biogas plants generate as much energy as two nuclear reactors (Statista, 2014).

1.2 Biogas Storage

While in practice most biogas is used as it is produced, biogas storage is useful when production exceeds consumption requirements or during maintenance of digester and engine equipment. For on-farm storage, the needed volume, possible corrosion and the cost must be considered when choosing a biogas storage system. Corrosion occurs due to hydrogen sulfide (H_2S), a colorless, very poisonous, flammable gas which is produced in small amounts by the anaerobic digestion or fermentation of biodegradable materials. Low-pressure storage tanks can be made of steel, fiberglass or flexible fabric. Biogas can also be stored at medium – and high-pressures (up to 140bar), but this requires that the H_2S has to be removed. High-pressure storage saves space, but is only economical when the biogas is upgraded from average 50% to 97% methane. This way, the energy needed for compression amounts to 17% of the energy content of the gas (Krich et al., 2005).
A well suited gas holder is the flexible inflatable membrane top, as it is integral to the digester and does not react with H_2S.

1.3 Storage with Membrane Solutions

Sattler AG is a manufacturer of hi-tech textiles, which among other products, are used for biogas storage systems (Sattler AG, 2012). Such biogas storage systems consist of an outer and an inner membrane (see Figure 2). The biogas is kept in the inner membrane, while the outer membrane holds the biogas storage in shape, regardless of how much biogas is currently stored, since the two membranes are kept apart by pressurized air.

A Outer membrane B Inner membrane C Air Flow System D Support air blower
E Anchor ring F Level meter
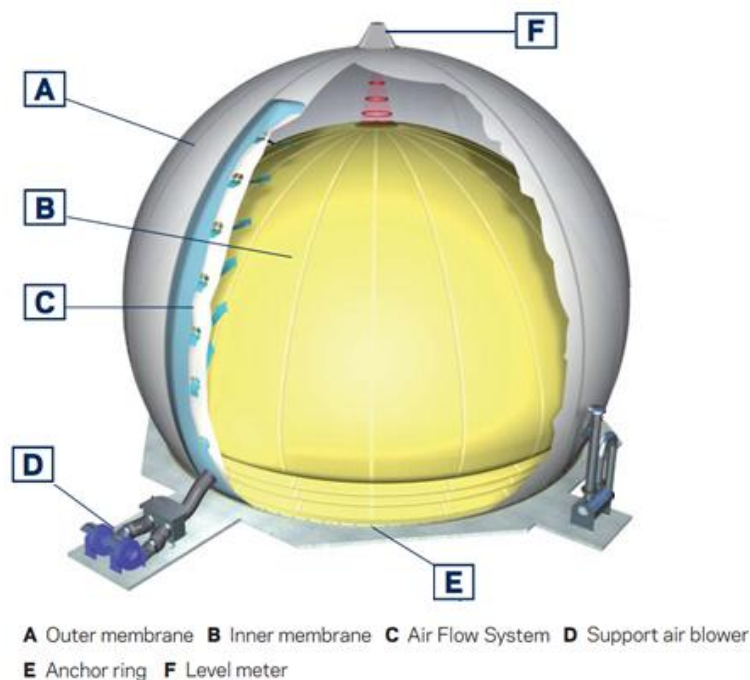
Figure 2: Design configuration of a ¾ spherical biogas storage system (Sattler AG, 2012)

Sattler AG produces two main shapes of such biogas storage systems – spherical shapes, held by air and conical shapes held by a mast (see Figure 3).

Figure 3: Different shapes of biogas storage tanks made by Sattler AG, conical (top left), ¼ sphere (bottom left) and ¾ sphere (right) (Sattler AG, 2012)

One main issue with biogas storage systems made of high-tech textiles, is that a spherical shape cannot be achieved by a two dimensional plane of base material without any distortion. Sattler AG produces the different geometries via welding of different cutouts. The tensile stresses acting on the welding seams are calculated with a finite element model.

This thesis looks into the difference between the real shape and the designed shape of a selected ¾ spherical biogas storage system. Therefore the whole surface of the ¾ sphere has to be measured. This will be called macroscopic view in this thesis.

1.3.1 Whole Shape

The macroscopic view deals with the overall shape of the biogas storage system, e.g. how well it approximates the design geometry. Uncertainties in the manufacturing and welding process and the distortion due to the curved planes lead to deviations from the design geometry, which can be seen near the welding seams. These welding seams are designed to withstand high tensile stress. This tensile stress depends upon curvature, where at the same pressure, lower curvature leads to higher tensile stresses. With bigger differences to a spherical shape, forces normal to the welding seam increase and can cause damage to the welding seam over time. These forces are calculated with a finite element model. Knowledge of the real geometry of the biogas storage system can help to improve the production process and the cutout layout.

1.3.2 Welding Seams

The welding seams in detail are also of interest, this will be called microscopic view in this thesis. For this purpose a test half-sphere with an approximate diameter of 1.2m is available at Sattler AG. Here the behavior around the welding seam as pressure increases should be measured.

1.3.3 Filling Level

Another interesting geometry of the biogas storage system is that of its inner membrane, since here the filling level can be measured. Depending on how much biogas is pumped into the storage, the inner membrane rises or folds inside the outer membrane, whilst pressurized air holds the macroscopic geometry of the biogas storage system.

1.4 State of the Art

Sattler AG has performed a measurement campaign to determine the macroscopic geometry of a spherical biogas storage system in the past. The approach of sigma3D GmbH used an optical measurement system (chapter 2.1.1.2), but no comparison to the finite element model was performed. Their visualization of the biogas storage system showed deviations to a sphere were highest at the welding seams and at the pole area where flattening occurs. Figure 4 shows the resulting visualization.
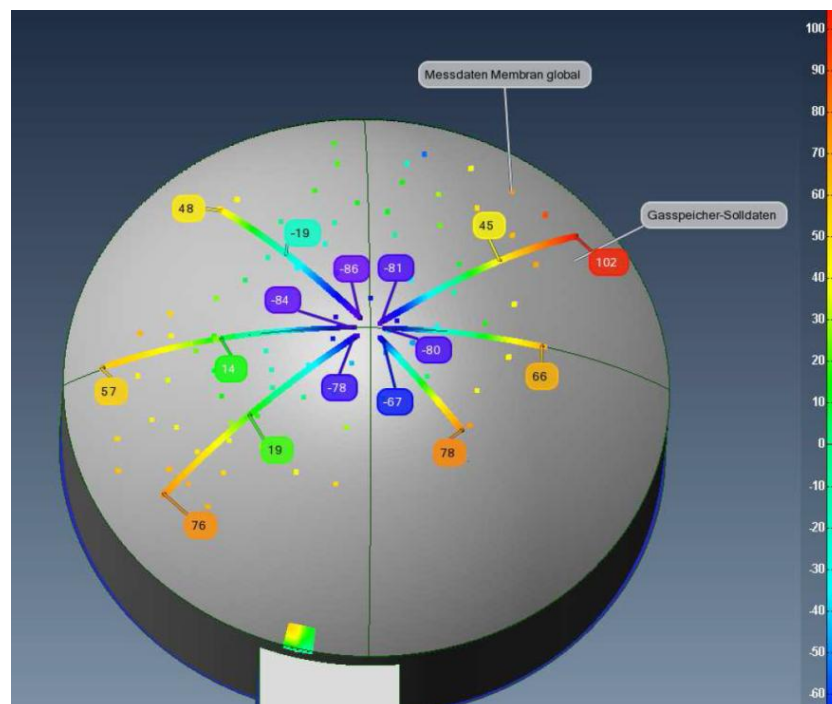
Figure 4: Visualization of differences to presumed shape in mm (Sattler AG, 2010)

There are a number of companies which specialize in 3D measurements of objects, most of which use laser scanners for bigger objects and structured light scanning systems for detailed recording of smaller objects.

As of now, the filling level is measured either via laser or ultrasonic distance measurement at top of the biogas storage system, or via one or multiple hydrostatic sensors. Because of the folding of the inner membrane, it is not possible to determine an accurate filling level from measurements of a small number of points. With better knowledge of the filling level, the efficiency of the biogas storage system can be increased by participating in spot market trading. In these virtual marked places, for example the European Energy Exchange, the spot market provides 24/7 trading for short-term optimization. This is only possible, with accurate knowledge of the filling level of the biogas storage system, since there are penalties for misdelivery involved (EEX, 2013).

1.5 Goals and Outline

The goals of this thesis are to explore different approaches for measuring the whole shape (macroscopic view), the change in the vicinity of the welding seams (microscopic view) and the current filling level (inner membrane) of a biogas storage system. These three tasks obviously have different requirements.

Industrial measurement systems and the field of geodesy offer a variety of technologies and methods for measuring 3D objects. Chapter 2 provides an overview of such technologies and methods and evaluates their suitability for the goals of this thesis.

After the theoretical review of different methods, one will be chosen and the chain from measuring to analysis and interpretation will be completed for the macroscopic view on a test object.

1.5.1 Requirements for the Macroscopic Measurements

The whole shape of the biogas storage system should be measured with a grid of about 10cm x 10cm, with a point accuracy of 1cm. The measurements must be contact-free, to avoid deformations due to the measurement process.
The test object is located in Rudersdorf, Austria. The ¾ sphere has a height of 5.5m and a diameter of 7.4m. Figure 5 shows the test object and its surroundings. The accessibility is partly limited and must be taken into account.

Figure 5: The previous ¾ sphere in Rudersdorf, Austria (http://gis.bgld.gv.at/)

A perfect 10cm x 10cm grid of the whole shape would result in approximately 13000 points. Figure 6 shows a schematic test object with a simplified point grid.
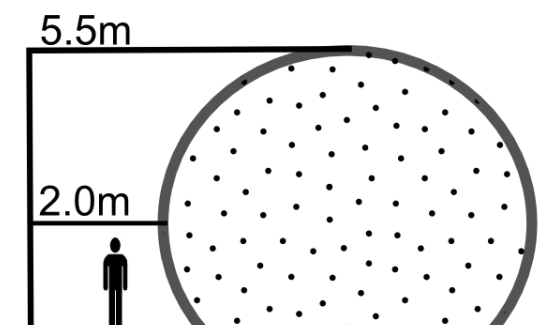
Figure 6: ¾ sphere with simplified point grid

When multiple approaches for measuring the whole shape of this test object meet the requirements, one must be chosen and tested in the laboratory on the fabric of the membrane. After that assessment, a measuring plan can be developed and implemented in the field. The result should be a point cloud. Sattler AG provides a reference point cloud of the finite element model. Commercial software will be used for the calculation of the point cloud difference. The interpretation of the results will be carried out in cooperation with Sattler AG.

1.5.2 Requirements for the Microscopic Measurements

For the measurement of the vicinity of the welding seam, the point grid has to be denser (5mm x 5mm and a point accuracy of 1mm). For this task, Sattler AG provides a different test object – a half-sphere with a diameter of approximately 1.2m. Here the area of interest covers the immediate vicinity of the welding seam, approximately 40cm x 120cm and results in at least 20000 points. This area should be measured every 10 seconds, since the goal is

to investigate the behavior of the welding seam while pressure increases. Certain aspects have to be taken into account, because the pressure in the test object will be increased until it explodes. This part will not be realized in this thesis.

1.5.3 Requirements for the Filling Level Measurements

To measure the current filling level of the biogas storage plant, the inner membrane must be measured. Current technologies for measuring the filling level measure single points on the inner membrane. This can lead to high deviations from the real shape, since the inner membrane folds and takes hard to predict shapes with different filling levels. This problem is shown in Figure 7.
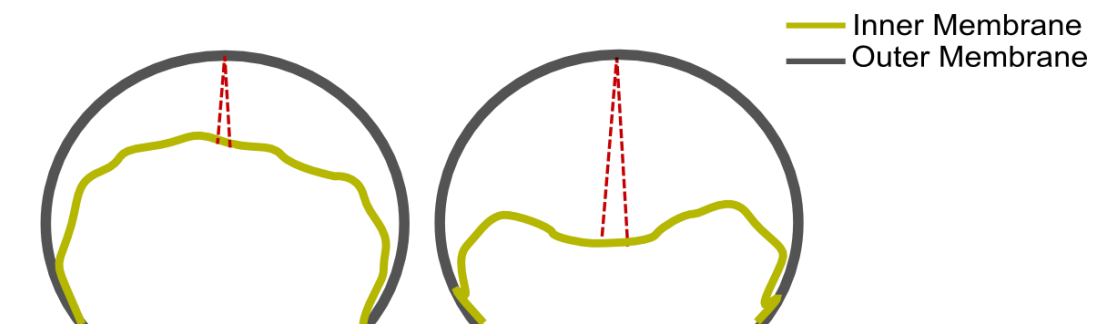
Figure 7: Schematic visualization of the inner membrane with different filling levels

The volume of the inner membrane should be determined with a maximum deviation of ±5% of the volume every 5 minutes. The measurements of the inner membrane will not be realized in this thesis.

2 Methodology and Technology

To provide an overview of current methods and technology, literature research was performed. Hereby geodetic textbooks and geodetic journals as well as literature from different fields such as metrology and brochures were reviewed. Since the approaches for the macroscopic view, microscopic view and the filling level measurement are quite different, they are discussed separately. Here the macroscopic view gains special focus, since the measurement of the whole shape of a biogas storage system should be performed.

2.1 Measurement Systems to Determine the Whole Shape

There is a number of promising measurement systems that can deliver 3D point clouds of large objects. In this chapter they are categorized in basic principles – image based, probe based and laser based systems. Figure 8 shows the discussed measurement systems.
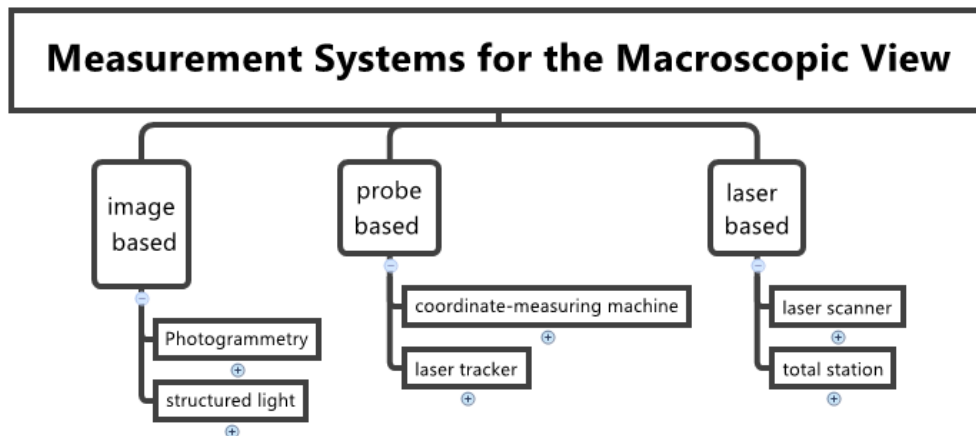
Figure 8: Overview of different measurement systems for the macroscopic view

To visualize the accessibility of the ¾ sphere a color coded sketch is made for each measurement system. Figure 9 shows an example of such a sketch, where green means easy access, orange means help is needed and red poses problems.
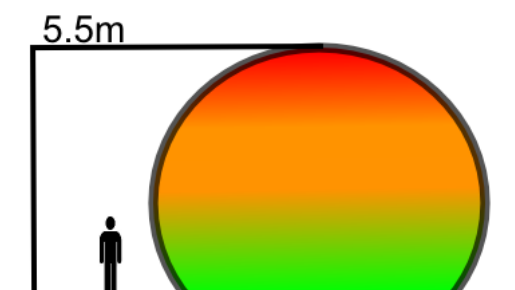
Figure 9: Color coded accessibility of the ¾ sphere

2.1.1 Image Based Systems

This chapter describes image based measuring systems. These systems utilize one or multiple cameras to derive 3D information from images.

2.1.1.1 Photogrammetry

Photogrammetry uses photographic images to reconstruct 3D objects. The basic principle is triangulation. The object is photographed from at least two locations, so that the same points on the object can be identified in the images. These lines of sight from the different camera positions to the object are intersected to produce 3D coordinates. This is basically the same as intersecting the lines of sight of two theodolites. In the case of theodolites, two angels are measured to generate a line of sight. If the positions of the theodolites are known, the intersection can be easily calculated. In the case of photogrammetry, the measurement is the 2D position of the object in the images. Therefore a single camera can capture a static scene from multiple setup points, or multiple cameras can capture a scene simultaneously. In any case the location and aiming direction of the camera must be known. Therefore the so called exterior orientation has to be calculated.

The interior orientation deals with image coordinates, since the center of the image sensor and the center of the camera will not perfectly coincide and corrections for radial distortion and refraction must be taken into account. The simplest mathematical model for interior orientation is a similarity transformation with the four parameters – translation in x and y, scale factor and the rotation angle. Since the measuring system is manufactured and as such is not perfect, the affine transformation is an improved mathematical model for the interior orientation. Here the scale factor is subdivided into x and y axis and the skew angle for non-perpendicularity is introduced. This leaves 6 parameters for the interior orientation (Schenk, 2005).

The exterior orientation is the relationship between image and object space. The location of the perspective center of the camera and its attitude in the object coordinate system is needed, this leaves six parameters – the coordinates x, y, z and three rotation angles. The image coordinates can be measured and the focal length is a calibrated constant, so every point leads to two equations, but adds three unknowns, namely the coordinates of the object point. To solve this equation system, there must be known points on the object, so called control points, which can be measured and marked for instance with a total station.

The bundle block adjustment is a widely used approach to solve the orientation of multiple images simultaneously. Here the multiple images must be overlapping, so that the images can be connected to a block. This way, all images can be oriented by using only three control points with additional tie points between the images. The coordinates of these tie points may be unknown and can be realized with automatic image matching methods. The term bundle refers to a bundle of light rays passing through the perspective center to the object points. The bundles from all images are adjusted simultaneously, so that the remaining errors at the tie points, control points and perspective centers are distributed and minimized (Aber et al. 2010). Figure 10 shows how such an image block can be realized.
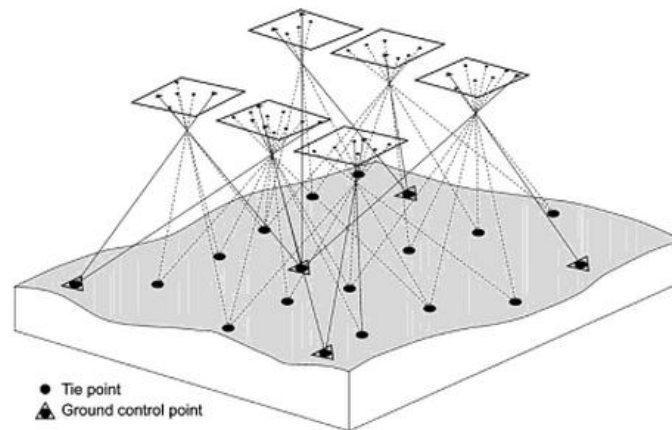
Figure 10: Principle of bundle block adjustment with ground control points and tie points (Gisbox, 2013)

The result of the bundle block adjustment is the orientation of all images as well as the coordinates of the tie points.

Photogrammetry represents a well-established measurement system for 3D objects. The measuring process is very fast and software for automated reconstruction is available. Figure 11 shows the approximate accessibility of the ¾ test object. Only the pole area cannot be reached from the ground. Therefore a lifting platform would be needed. With photogrammetry vibrations should pose no problem, since the image is taken almost instantly.
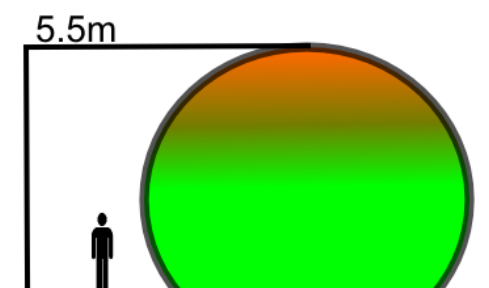
Figure 11: Accessibility with photogrammetry

However the texture of the outer membrane poses a significant problem, since object points must be detected in multiple pictures to triangulate the coordinates. Poor texture leads to problems in the image matching process and causes artifacts.

Table 1: Advantages and disadvantages of the photogrammetry

Advantages	Disadvantages
non-intrusive	reference frame required
high spatial resolution	low texture leads to artifacts
fast measuring process	markings necessary
simultaneous capturing of many points	

2.1.1.2 Structured Light Photogrammetry

Optical measurement systems are an extension to photogrammetry. Figure 12 shows the ATOS III optical sensor. It uses two fixed cameras combined with a light projector in the center. Due to the fixed positions of the cameras the relative orientation is known by calibration from the manufacturer.
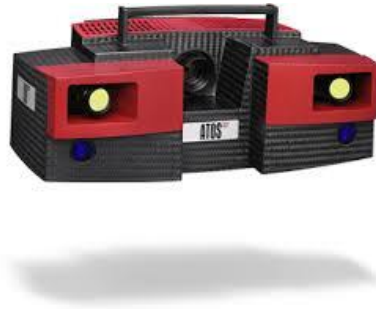
Figure 12: ATOS III optical sensor (Gom, 2013)

3D optical measurement systems usually project periodically light patterns which are sequentially shifted across the object. A point cloud can then be measured via classical photogrammetric methods, with the advantage of better texture of the object due to the light projections. Marking of the object is still required, since the optical sensor needs to be oriented relative to the object so that the acquired point clouds are in a common reference frame (Mazaheri et al., 2008).

Another approach of object reconstruction is deflectometry. This is a radiometric approach where the measurements are intensities. The projected light patterns are measured with the cameras. Due to curvature of the object, the reflected image of the light patterns is distorted. Since the projected light patterns are known, the curvature can be calculated in every point of the object (Kammel, 2004).

Figure 13 shows the accessibility with 3D optical systems. Same as with photogrammetry, a lifting platform would be needed to reach the pole area.
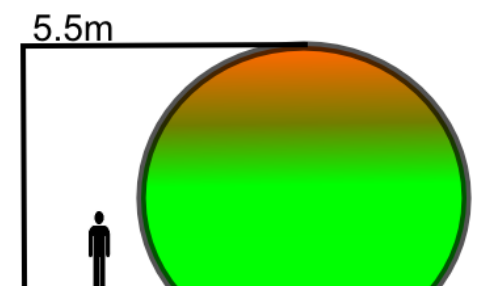
Figure 13: Accessibility with 3D optical systems

Table 2: Advantages and disadvantages of structured light photogrammetry

Advantages	Disadvantages
non-intrusive	Reference frame required
high spatial resolution	Markings required
fast measuring process	

2.1.2 Laser Tracker

Laser trackers lock on a target, usually a sphere with a reflector, and follow this target as horizontal and vertical angles as well as the distance are measured. The distance measurement uses interferometry and therefore achieves very high accuracy up to 60µm. Modern laser trackers can measure absolute distances as well, by integrating a second distance measurement unit with absolute distance measurement capabilities (Hexagon, 2008). Figure 14 shows as example a laser tracker from Faro.

Figure 14: Faro Laser tracker ION (Faro, 2013)

The target is then moved over the object, while the laser tracker continuously follows and measures the target. If the line of sight is interrupted or the signal is lost for any other reason, the system must be reinitialized, unless it can measure absolute distances.

Laser trackers are widely used in industrial manufacturing, but the target needs to touch the object, which is why it does not meet the requirements discussed in chapter 1. Figure 15 shows the accessibility of the test object. Up to 2m of height the sphere could be easily reached, for higher positions additional equipment would be needed.
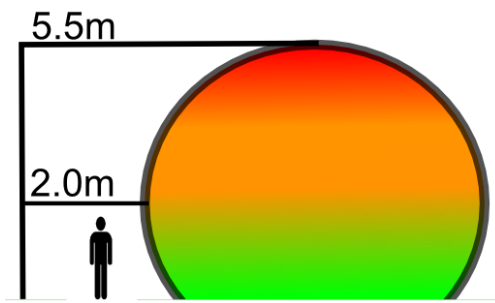
Figure 15: Accessibility of the test object with a laser tracker

Table 3: Advantages and disadvantages of the laser tracker

Advantages	Disadvantages
high accuracy	slow measuring process
	target is moved along object by hand
	difficult to realize a grid
	intrusive

2.1.3 Coordinate measuring Machine

Coordinate measuring machines (CMM) are widely used in quality control of many manufacturing processes. The CMM consists of three axis, which represent a coordinate system and a touch probe, that can be moved along the three axis. The test object is placed on the CMM, and the coordinates are recorded as the probe hits the object. There are a variety of different CMM sizes and probe types available. Figure 16 shows a CMM.

Figure 16: Coordinate measuring machine (Directindustry, 2013)

As the object has to be put on the CMM, this measurement system is not suited for the macroscopic view. The small test object for the microscopic view would fit onto a CMM, but as the measurement process only measures a few points per minute, it does not meet the requirements.

Table 4: Advantages and disadvantages of coordinate measuring machine

Advantages	Disadvantages
high accuracy	not mobile
common reference frame	slow measuring process
	limited size

2.1.4 Laser Scanner

Laser scanners perform very fast measurements of 3D objects with high spatial resolution and accuracies in the range of millimeters. Laser scanners are used in a variety of fields and can be mounted on different platforms.

- a) tripods, pillars
- b) cars, trains
- c) aerial platforms

Tripods and pillars are used for deformation measurements and monitoring. Movable ground platforms such as cars or trains are used for mobile mapping applications. Figure 17 shows a laser scanner from Zoller & Fröhlich (ZF) as it is mounted on a tripod. From this point, the instrument measures horizontal and vertical angles as well as the distance to a point. The user can set the angle steps the laser scanner takes, as the instrument rotates and thereby collects a 3D point cloud of its surroundings.

Figure 17: Zoller & Fröhlich (ZF) Imager 5010 (Zoller & Fröhlich, 2013)

Since the measurements do not require reflectors, marking of the object is not necessary. Modern laser scanners can deliver up to 1 million points per second, so the measuring process is very fast.

If multiple setup points for the laser scanner are required to scan the whole object, the point clouds must be transformed into a common reference frame. This can be achieved by setting up the scanner on known positions or by registration of the point clouds via recognizable targets (Eling, 2009).

Important parameters in laser scans are point density and spot size. For each application a suitable laser scanner must be found. Lindstaedt et al. (2011) compared four different laser scanners under the same conditions. Table 5 shows the technical specifications of these laser scanners.

Table 5: Technical specifications of four different laser scanners (Lindstaedt et al., 2011)

	Leica C10	Riegl VZ400	Faro Photon 120	ZF Imager 5006i
Range	300m	600m	120m	60m
Distance measurement	Impulse	Impulse	Phase	Phase
Measurement rate	50.000pts/s	976.000pts/s	125.000pts/s	500.000pts/s
distance accuracy	4mm at 50m	2mm at 25m	5mm at 100m	6mm at 50m
Angle resolution	0.0023°	0.009°	0.0005°	0.0018°
3D point accuracy	6mm	Not specified	Not specified	10mm at 50m

A laser scanner can cover most of the ¾ test sphere, but at the pole area the laser beam hits at a very low angle and this can lead to higher errors in the distance measurement. This can be solved with an additional setup point on a nearby rooftop, since a lifting platform will most likely be too unstable. Figure 18 shows a sketch of the accessibility.
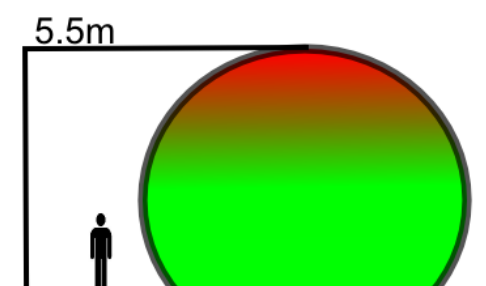
Figure 18: Accessibility with a laser scanner

Table 6: Advantages and disadvantages of the laser scanner

Advantages	Disadvantages
non-intrusive	reference frame required
high spatial resolution	outlier filtering required
fast measuring process	thinning of the point cloud

2.1.5 Total Station

A modern total station is a very flexible measuring instrument, used in surveying, civil engineering and construction. Similar to a laser scanner, the horizontal and vertical angles as well as the distance to a point are measured. The distance measurement uses electro-magnetic waves and can be calculated with the time of flight of an impulse. Another way is to send out modulated laser phases and measure the phase shift. To solve the ambiguities, different modulations must be sent until the phase shift is accurate enough. These polar measurements can range up to a few kilometers when using a reflector, but will also measure distances up to a few hundred meters in reflectorless mode.

Classic tachymetry usually targets first to known points and determines the setup point of the total station. Then either new points can be measured, or coordinates can be marked in nature. When measuring at different epochs, differences can be calculated in-field for monitoring applications.

In the last few years total stations have expanded their capabilities by including cameras, automated target recognition (ATR) and faster measuring modes. Cameras allow image measurements in post-processing, ATR enables tracking of moving targets and finding reflectors for monitoring applications. Faster measuring modes, in case of the in Figure 19 shown Leica Nova MS50 up to 1000 points per second, allow the total station to perform scans similar to a laser scanner.

Figure 19: Leica Nova MS50 (Leica, 2013a)

Figure 20 shows the accessibility of the ¾ test object with a total station. Near the pole area the angle becomes increasingly low and can lead to bigger errors in the distance measurement. This can be avoided when using a lifting platform, but vibrations might influence the measurements. Therefore an additional setup point on a rooftop in the vicinity of the sphere would be a better solution.
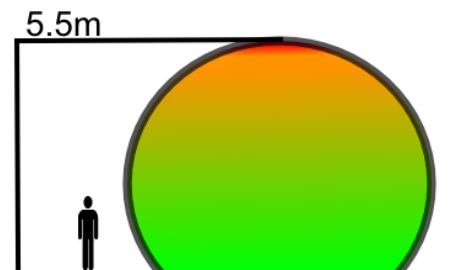
Figure 20: Accessibility with a total station

Table 7: Advantages and disadvantages of the total station

Advantages	Disadvantages
non-intrusive	more customization leads to more preparation work
flexible spatial resolution	
remotely controllable	
creates reference frame	

2.2 Volume Determination

Determining the volume of the inner membrane can be difficult for several reasons. As pressure decreases, the inner membrane lowers itself irregularly. Due to the complex geometry it is very hard to predict the shape of the inner membrane with different filling levels, since asymmetric shapes are common. Also condensed water may accumulate and drop on the inner membrane, leading to donut shapes.

To measure the volume accurately to +/- 5%, an approach which uses an area based system seems necessary. The measurement system must also be industrial-suited and therefore withstand harsh environmental conditions. Additionally it must be safe to use in biogas surroundings.

2.2.1 Cable Level Systems

Cable level systems are commonly used in silo measurements as they are easy to install and have a low price. The system currently in use by Sattler AG is shown in Figure 21. It is mounted on top of the biogas storage and connected with the inner membrane. The volume is then deduced from the length of the cable.

Figure 21: Cable level system (FSG, 2013)

With multiple cable level systems more points can be measured, which would increase the reliability.

Table 8: Advantages and disadvantages of cable level systems

Advantages	Disadvantages
not affected by angle of incident	single point measurement
easy to install	intrusive
very durable	
explosion proof designs available	
field repairable	

2.2.2 Ultrasonic

Ultrasonic measurements use sound waves to measure distance. An ultrasonic signal is sent out by the transmitter and picked up by the receiver. When the signal is interrupted in some way, for example when hitting the inner membrane, it leads to a signal change. The footprint depends on the opening angle of the ultrasonic system (US) as shown in Figure 22.
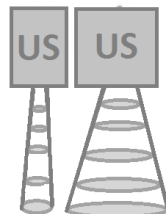
Figure 22: Different footprints of ultrasonic measurement (US) systems

There are no moving parts in ultrasonic systems and thus maintenance is minimal. Ultrasonic systems are currently used by Sattler AG, but they measure the inner membrane only on single points.

3D ultrasonic measurement systems are currently being developed in the field of medicine to replace computer tomography. In this application multiple sensors (up to 48 sensors with 2000 ultrasound transducers) are arranged in a cylinder. These sensors generate huge amounts of data which can be used to generate 3D images (Schwarzenberg, 2008). Unfortunately this technology is not yet suitable for industrial application.

Table 9: Advantages and disadvantages of ultrasonic systems

Advantages	Disadvantages
non-intrusive	system is affected by changes in the angle of repose
dynamic measurements	single point measurement (industrial)
easy to install	

2.2.3 Guided Wave Radar

Guided wave radar uses radar waves, which propagate along a probe. This system is commonly used in liquid storage systems. For example in an oil-water separator, there will be three reflections measured. First the reflection from the air-oil surface, next the reflection of the oil-water interface, and last a reflection from the end of the probe. There is a minimum distance required, so the top of the probe is a dead zone. Since there is always a reflection from the end of the probe, the end also represents a dead zone (Smith, 2009).

Guided wave radar cannot be applied to measuring the inner membrane, since it penetrates the membrane. Additionally it represents a single point method and is thus not desirable.

Table 10: Advantages and disadvantages of guided wave radar

Advantages	Disadvantages
dynamic measurements	probe must go through silo
multiple reflections	single point measurement

2.2.4 Thru-Air Radar

Thru-air radar (TAR) exists in two basic forms – pulsed radar and FMCW (frequency modulated continuous wave). It uses higher powered waves then guided wave radar to

penetrate dust and generate higher signal-to-noise ratios. Unfortunately this also penetrates the inner membrane, since TAR is meant for bulk solid silos.

Table 11: Advantages and disadvantages of thru-air radar

Advantages	Disadvantages
non-intrusive	requires material with a dielectric constant > 1.8
dynamic measurements	multipath possible
high accuracies	

2.2.5 Laser Level Systems

Laser level systems depend on the accurate detection of the time-of-flight of a laser pulse to travel to the object and back. The principle is the same as with a laser scanner, only no angles are measured and therefore it is a single point measurement system.

New laser level systems like the VM3D from ABB as seen in Figure 23 feature a movable laser. This system represents a small scale laser scanner and can measure multiple points in a short time (ABB, 2013).

Figure 23: 3D laser level system VM3D from ABB (ABB, 2013)

Table 12: Advantages and disadvantages of laser level systems

Advantages	Disadvantages
non-intrusive	angle of incident may influence signal
easy to install	
3D measurements	
robust	

2.2.6 Industrial Tomography

Computer tomography (CT) scanning is a well-established technology in medicine and can also be used in industrial applications. Basically x-rays are emitted at an object and hit either an array detector or line detector after passing through. Step-by-step rotation leads to a series of two-dimensional images. The CT image is then reconstructed using three-dimensional filtered back projection. Figure 24 shows a CT system for samples up to 1m in diameter, which counts as a large sample (GE, 2010).

Figure 24: phoenix vtomex L 450 (GE, 2010)

Table 13: Advantages and disadvantages of industry tomography

Advantages	Disadvantages
non-intrusive	high cost
multiple point measurement	small objects (1m diameter)
3D reconstruction of object	

2.2.7 Photometric Stereo

Photometric stereo is a technique in computer vision. It determines the surface normal by taking photographs under different lighting conditions while holding the viewing direction constant. For many surfaces, the fraction of the incident illumination reflected in a particular direction depends only on the surface orientation. The idea of photometric stereo is to vary the direction of incident illumination between successive views. For every point in the image the difference in illumination is considered, and the surface normal calculated. In the case of two images, there is still ambiguity for every point. Therefore three differently illuminated images are needed. Another condition is the diffuse reflection of light from the object, since shiny spots lead to errors (Handschuh, 2009). Figure 25 shows a hand which was reconstructed with photometric stereo using three images.
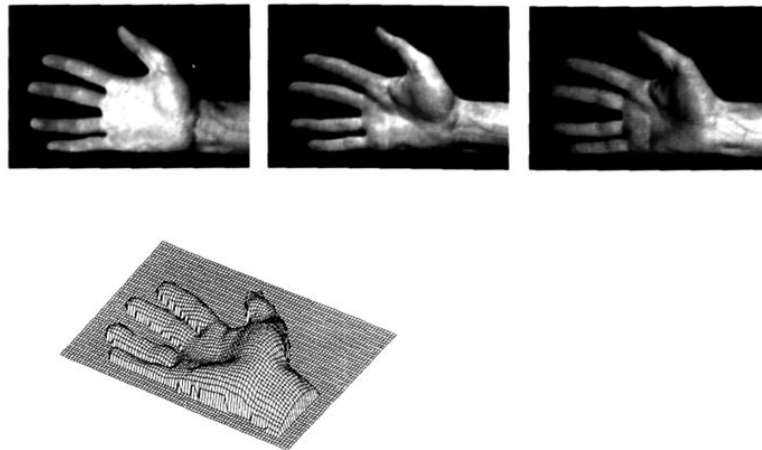
Figure 25: Three differently illuminated images and the reconstructed 3D model (Bader, 2001)

Table 14: Advantages and disadvantages of photometric stereo

Advantages	Disadvantages
non-intrusive	customized solution must be found
multiple point measurement	
3D reconstruction of object	
works best on smooth surfaces	

2.3 Evaluation and Recommendation

In this chapter the measurement systems which meet the requirements for each application are compared to each other, so that the most suitable may be recommended.

2.3.1 Recommended Measurement System to Measure the Whole Shape

For the macroscopic view, the requirements are met by a laser scanner, photogrammetry, the optical system and the total station.

- Photogrammetry: The insufficient structure of the membrane would require extensive markings on the whole object.
- Structured Light: This optical system would still require some markings on the object to connect the different measurements.

This leaves the laser scanner and the total station as viable systems. Since these systems operate in a very similar way, they can be compared directly.

An approximate measuring plan for the whole shape for both systems would require several setup points, to cover the whole shape. This leads to several point clouds that have to be

fused into one. This can be done either via point cloud registration, which requires setting up detectable reference points or via realization of a local coordinate system. The major advantage of a laser scanner is its very fast measuring speed, but since the object in question is rather small, the total station would not take much longer. Additionally, a total station can quite easily establish a local coordinate system, so that the individual scans could be fused into one in the field and no post-processing of the data would be required. Laser scanners usually need time consuming post-processing to register the individual scans.

For these reasons, the measurement system most suited for measuring the whole shape is a modern total station.

2.3.2 Recommended Measurement System for the Microscopic View

For the microscopic view, the requirements are met by photogrammetry and the optical system. Photogrammetry could be realized, when a grid of spots is glued onto the test object to provide better texture. But since the optical system can also capture the whole object at once, and thus does not require any marking, it seems to be the easier solution.
If the test object is inflated in slow steps, the laser scanner and total station could also measure the microscopic view, even if the whole scene is not captured simultaneously.

2.3.3 Recommended Measurement System for Measuring the Filling Level

To determine the volume of the inner membrane with higher accuracy, an area based measurement system must be found. Only the laser scanner and photometric stereo achieve this.
The laser level system VM3D from ABB is produced specially for silo measurements and should be able to measure the inner membrane every 5min, as are the requirements. Before it can be incorporated, it must measure the outer membrane from the inside, so that it does not make false detections.
Photometric stereo could measure the inner membrane a lot faster, but a customized solution must be produced. Since the light sources should not be too close together, it is also more difficult to install. Finally, if a solution is found, it should be producible in large quantities and be industrial robust. This means the initial cost of developing such a system could be relatively high. On the other hand, a camera, three light sources and a computer might be a lot cheaper than the laser level system VM3D from ABB.
For the final decision the following should be considered.

- What is the approximate development cost of a photometric system?
- What is the approximate cost difference between the two systems?
- Are high accuracies needed in every biogas storage system?

2.3.4 Conclusion and Next Steps

With the conclusion of the literature research, the goals of exploring theoretical solutions for measuring the microscopic view and the filling level have been reached. To implement the chain from measuring the whole shape of a test object, to analysis and interpretation, the literature research recommends the total station as a measurement system. Before an actual measuring campaign can be started, this recommendation has to be evaluated in the laboratory. For this purpose, Sattler AG provided a cutout of the membrane used with biogas storage systems, so that the laboratory testing can proceed on the actual material.

Only after approving the total station as a measurement system for the whole shape, the test object in Rudersdorf can be measured.

3   Laboratory Testing

This chapter deals with the testing of the total station Leica MS50. The MS50 has an angular accuracy of 1'' (0.3mgon) standard deviation ISO 17123-4 (Leica, 2013b). The manufacturer specifies for reflectorless distance measurements an accuracy of 2mm + 2ppm. This presupposes overcast, no haze, no heat shimmer and the object in shade. The specified surface is a Kodak Grey Card (90% reflective). To give a confident assessment of the accuracy of the measurements, the system has to be tested on the material of an outer membrane. For this purpose, several experiments have been set up. The MS50 can operate in three different measuring modes – single mode, dynamic mode and scan mode.

The single mode measurement is the most precise mode. A single measurement takes typically between 1.5s and 4s, depending on distance and surface reflectivity. The MS50 returns the distance with a resolution of 0.1mm.

In the dynamic mode, the MS50 is measuring the distance continuously with a typical rate of 7Hz - 8Hz. In this mode, the resolution of the distance is 1mm.

For the scan mode, the MS50 needs a defined scan field. This can be done by defining a rectangle with two points. A vertical resolution of 1mm and horizontal resolution of 2cm was chosen. This way, every scan consists of several vertical lines, while only the first is utilized. The scan files are stored on the SD Card onboard the MS50 and are converted into text files for further processing in Matlab.

3.1   Impact of Incident Angle on Surface Measurements

The incident angle is defined in Figure 26. This means orthogonal measurements have an angle of incidence of zero.
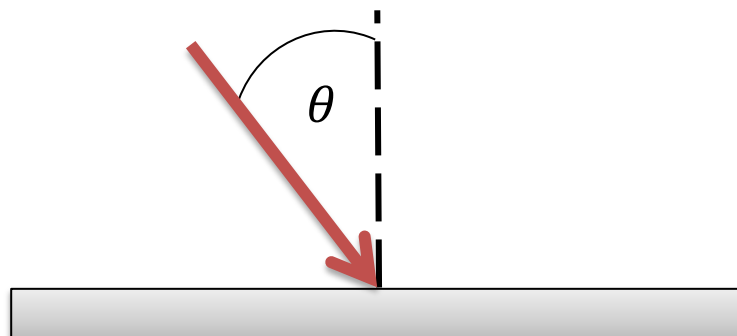
Figure 26: Definition of angle of incident (θ) to surface. The red arrow represents the laser beam of the MS50

For testing the accuracy of the reflectorless distance measurement for different angles of incident, a cutout of the membrane material has been mounted on a motorized theodolite TM1100. To align the MS50 laser beam orthogonal to the membrane, 25 evenly spaced out points were measured on the membrane. After fitting a plane using least squares adjustment, the angle between the laser beam and the surface model could be computed. Adjusting the

theodolite with this angle gave this test its starting position. Figure 27 shows an illustration of this experimental setup.
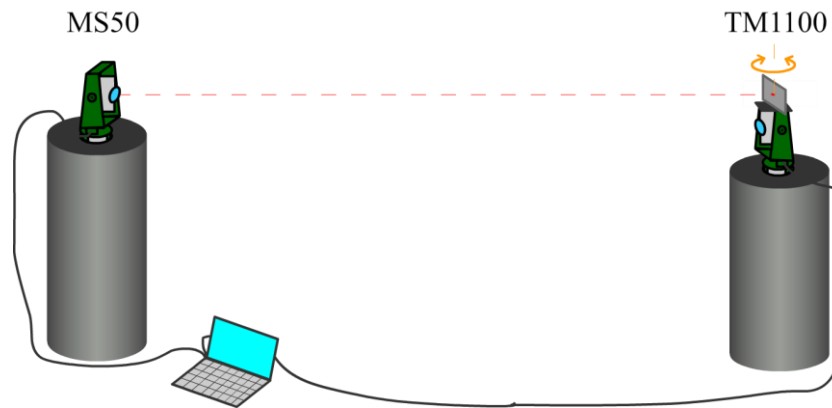
Figure 27: Experimental setup for angle of surface tests

Using a laptop and Geocom connection, the TM1100 was remotely rotated from -90gon to 90gon in 5gon steps, while distance measurements with the MS50 were carried out every step. To reduce random noise, 10 measurements were taken for every step in each measuring mode. After the TM1100 reached 90gon it changed direction to see if any hysteresis occurs. Since the TM1100 was rotated twice for 180gon in 5gon steps, 370 measurements were taken with each measuring mode.

This test was setup for the distances 5m and 12m, since those are the approximate distances that will be measured in the field (see chapter 4).

3.1.1 Analysis of Incident Angle Experiments

The TM110 was rotated twice for 180gon, once forward from -90gon to 90gon and once from 90gon to -90gon (return). In Figure 28 the forward and return measurements can be seen.
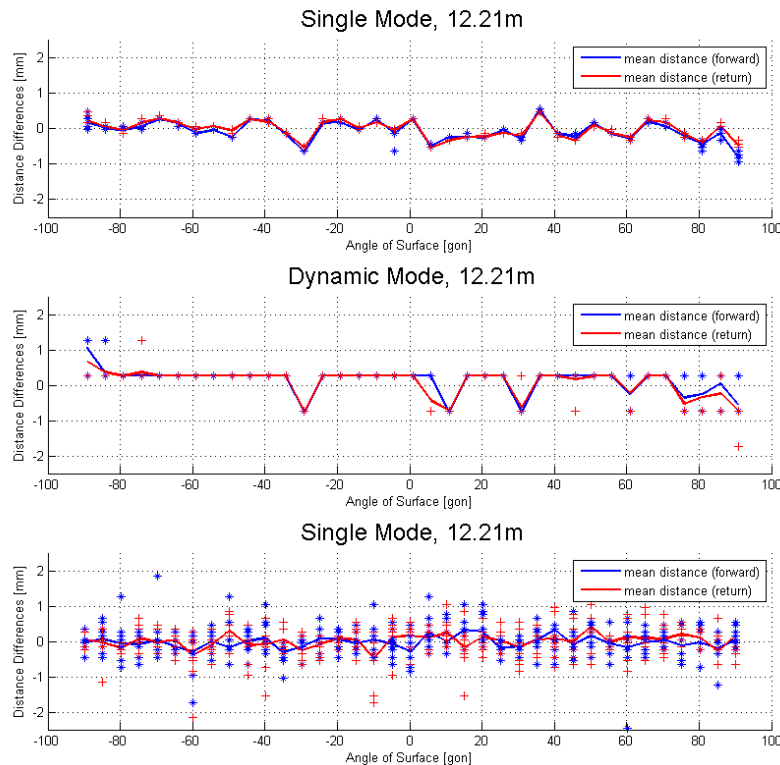
Figure 28: Data from incident angle experiments. The forward and return measurements can be seen separately

Since no hysteresis can be seen in Figure 28, the 20 measurements were averaged for every 5gon step. In Figure 29 the data from the 5m distance measurements is shown. Figure 30 contains the data from the 12m distance measurements. The average measured distance for every 5gon step is shown with a green line. The individual measurements are also plotted. Additionally the empirical standard deviation is plotted beneath each scan mode.

The single mode measures with a resolution of 0.1mm and is the most accurate mode. In the dynamic mode, the resolution of the MS50 is reduced to 1mm. Therefore the empirical standard deviation can also be zero, since many of the individual measurements show the same distance.

The scan mode can only be used when defining a scan area. Therefore a scan area was chosen, starting in the rotational axis of the TM1100 with an area of approximately half of the mounted membrane surface. The horizontal resolution was set to 2cm, while the vertical resolution was set to 1mm. This setup results ins scans with 4 vertical lines of points with a resolution of 1mm. For the incident angle test only the line in the rotation axis of the TM1100 is used. The distance in the middle of this line is then further used for the comparison in the different angle steps. At a first glance at the data, it can be seen that the scan mode has again higher resolution, but also higher spread of the individual distances.
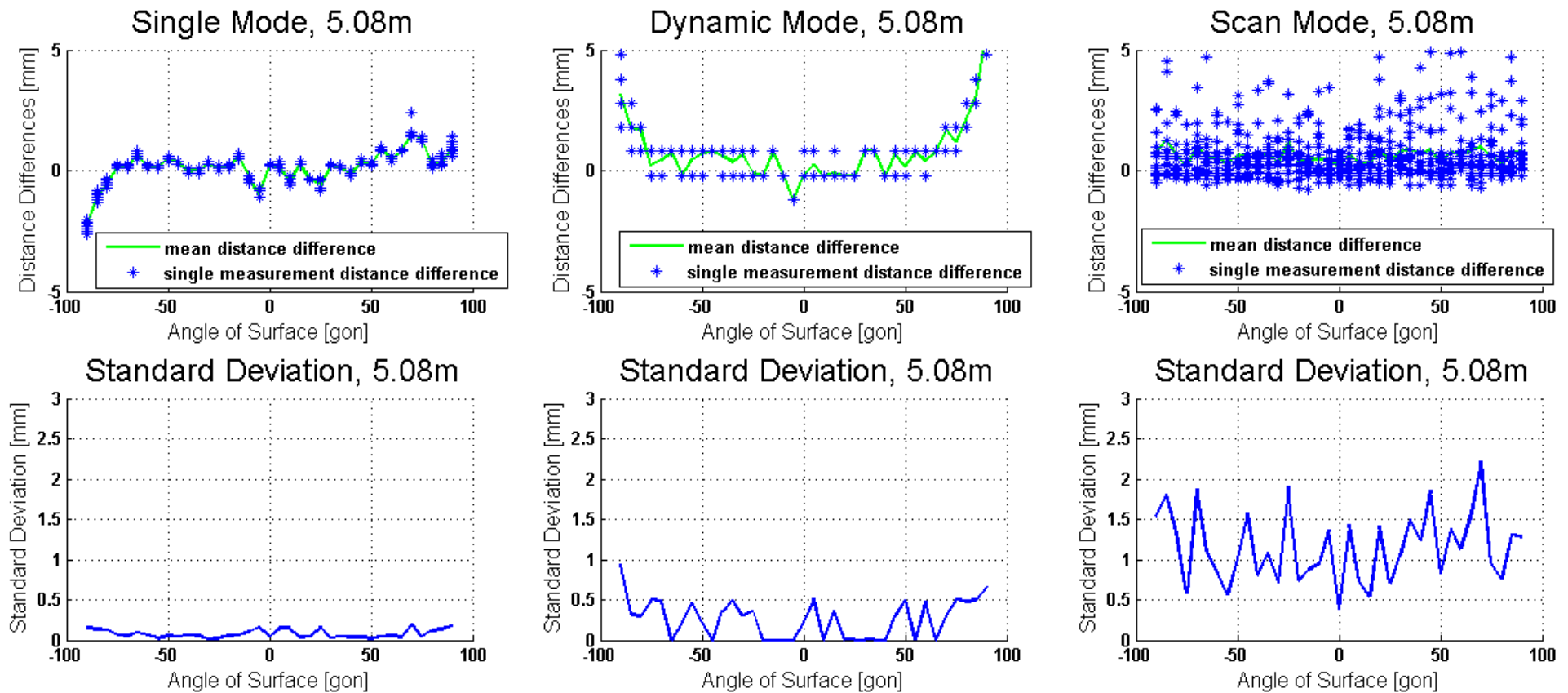
Figure 29: Impact of incident angle to surface on single, dynamic and scan mode distance measurements in a distance of approximately 5m
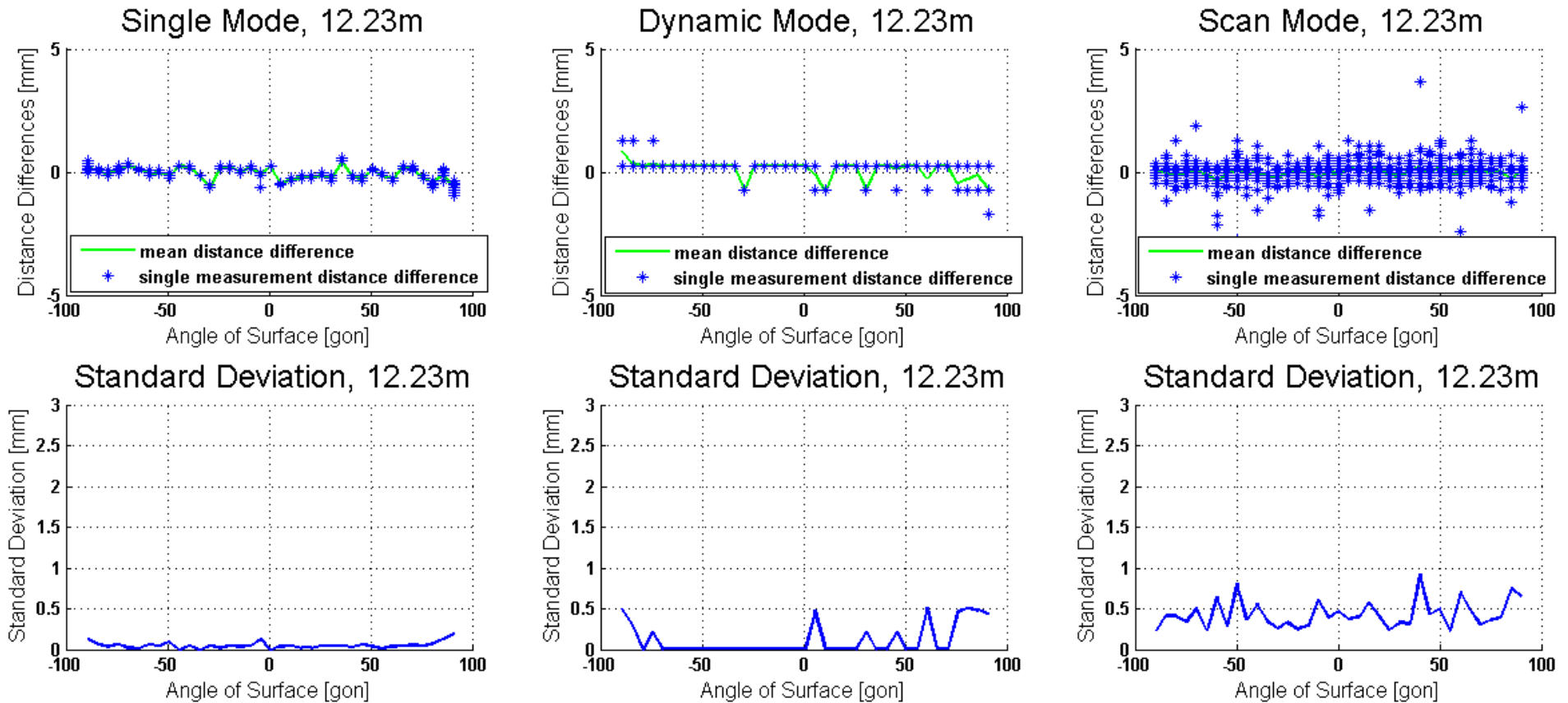
Figure 30: Impact of incident angle to surface on single, dynamic and scan mode distance measurements in a distance of approximately 12m

3.1.2 Results of the Incident Angle to Surface Experiments

When comparing the data in Figure 29 and Figure 30, the distances with approximately 12m have a lower standard deviation. Even at +/-90gon, where the standard deviation rises significantly for the approximately 5m distances, in approximately 12m distance the MS50 still gets reliable measurements.

Table 15 shows the overall standard deviations from incident angle experiments. Here the empirical standard deviations must be considered carefully, since the measurements are highly correlated and cannot offer any information on absolute accuracy.
Again, the approximately 12m distance measurements have lower standard deviation.

Table 15: Overall standard deviations for the incident angle to surface experiments

	Single Mode	Dynamic Mode	Scan Mode
STD 5m distance	0.68 [mm]	1.32 [mm]	1.24 [mm]
STD 12m distance	0.27 [mm]	0.41 [mm]	0.48 [mm]

3.2 Structure of Membrane

Since the membrane has an underlying woven structure, the influence of this structure on the distance measurement was also tested. Again a cutout of the membrane was mounted on the TM1100, which in turn was mounted on a shifting apparatus. To adjust the shifting apparatus orthogonal to the laser beam, it was measured on both sides using a mini prism. The shifting apparatus was then rotated slightly until both distances were the same. As in chapter 3.1 described the membrane was adjusted orthogonal to the laser beam.
The TM1100 was then shifted sideways from 0mm to 40mm in 2.5mm steps. The experimental setup is illustrated in Figure 31.
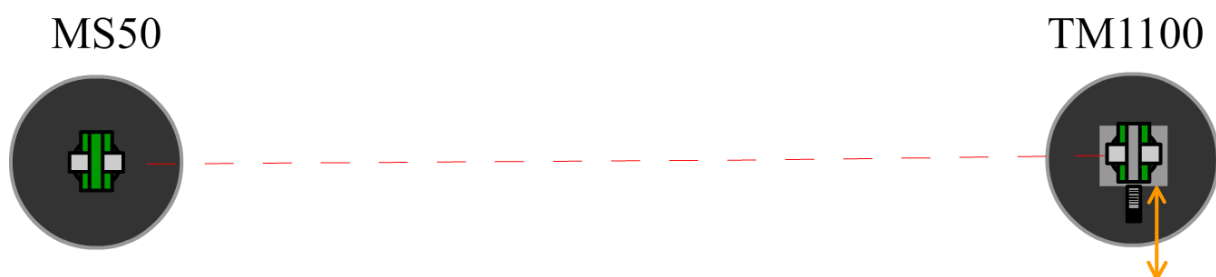

Figure 31: Illustration of experimental setup for testing of the membrane structure

Figure 32 shows the resulting distances plotted against the shift distance. A small trend (approximately 1mm) can be seen in the data. This could result from an imperfect alignment of the shifting apparatus. An offset of 1mm would be caused, when the shifting apparatus is not orthogonal by 1.5gon. Since the apparatus was adjusted by distance measurements on

both sides, this offset could occur when the distance on both sides is off by 0.5mm. Therefore this trend cannot be contributed to the structure of the membrane.

Again the scan mode shows a higher spread between individual measurements.
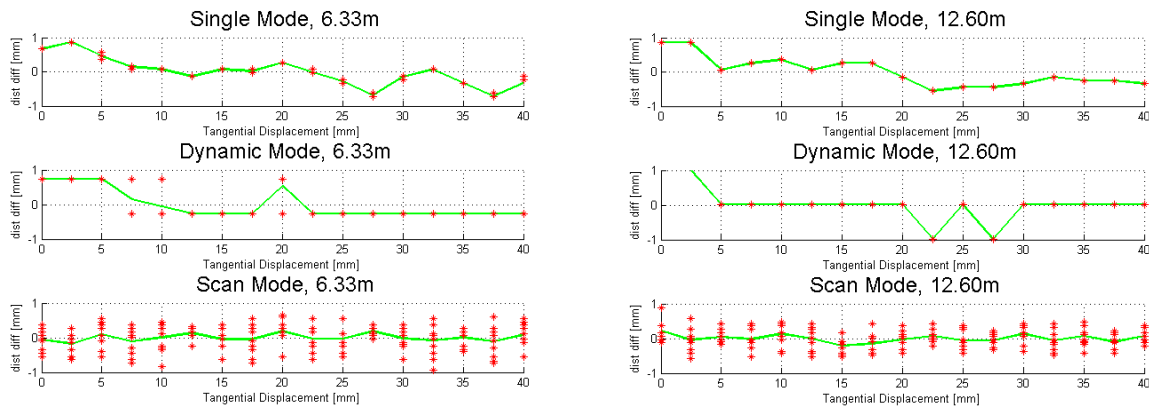

Figure 32: Influence of the membrane structure on distance measurements, for distances of approx. 6m (left) and 12m (right)

The empirical standard deviation for the membrane structure experiments can be seen in Table 16. Again the measurements are highly correlated.

Table 16: Overall standard deviations for the membrane structure experiments

	Single Mode	Dynamic Mode	Scan Mode
STD 6m distance	0.43 [mm]	0.44 [mm]	0.35 [mm]
STD 12m distance	0.41 [mm]	0.46 [mm]	0.28 [mm]

3.3 Resolution of Scan

As a final test the cutout of the membrane was scanned with a resolution of 1mm x 1mm. Afterwards another cutout of the membrane containing a welding seam was scanned with the same resolution. The two resulting point clouds were compared to see if the scan mode can detect the welding seam. This test was performed at a distance of 10m and the resulting point cloud differences are shown in Figure 33.
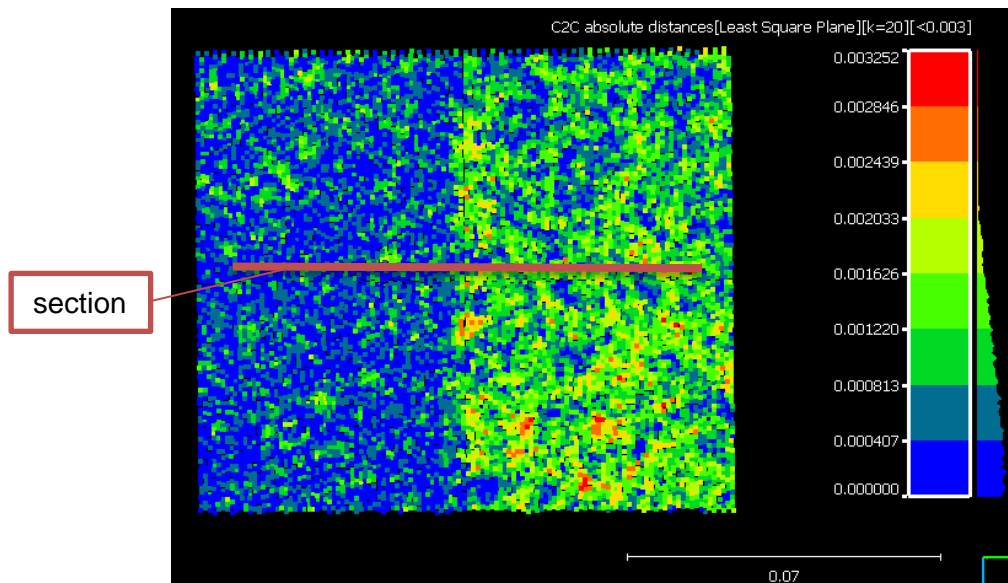
Figure 33: Point cloud differences between membrane cutouts with and without welding seam (unit of scale bar [m])

To detect the thickness of the welding seam, a section across the welding seam (red line in Figure 33) can be seen in Figure 34.
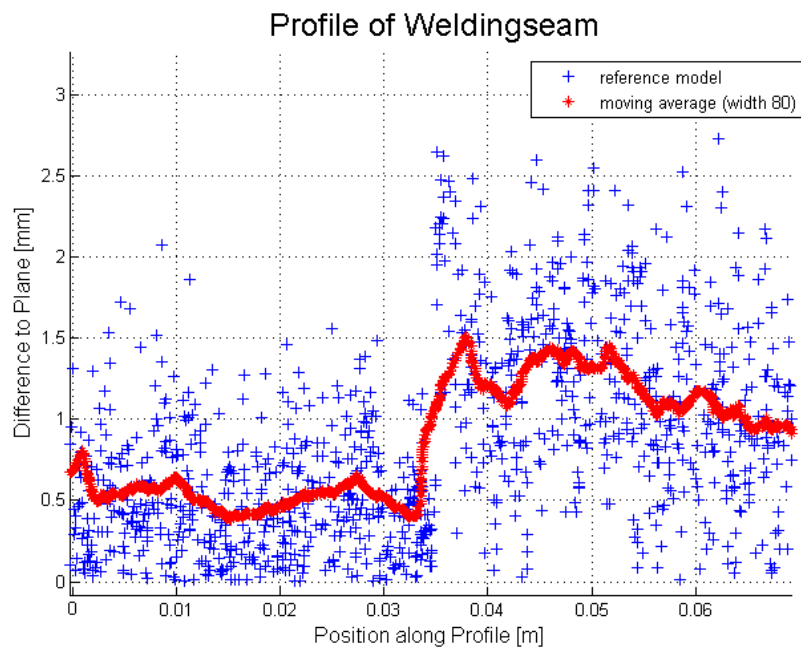

Figure 34: Profile across the welding seam. The scan data is shown in blue. A moving average of 80 scan points is visualized in red

From the filtered data the thickness of the welding seam can be seen, which is approximately 1mm.

3.4 Evaluation of the Measurement System

The laboratory tests of the Leica MS50 shows, that the measurement of a biogas storage system can be performed under the requirements set in chapter 1.5.1. The membrane shows good reflectivity, which is important for reflectorless measurements, whereas the structure of the membrane does not significantly affect the distance measurements. The inclination angle between the laser beam and the surface can be up to 80gon and still deliver reliable results.

4   Measurement with the MS50

In this chapter the measurement of the ¾ test sphere in Rudersdorf at the Sattler AG production facilities is described. The measurements were carried out on the 16.10.2013 between 9:00am and 16:00pm.

4.1   Field Plan for the ¾ Test Sphere Measurements

Before any measurements could be made, the setup points for the MS50 had to be chosen. As shortly described in chapter 1.5.1, the accessibility around the ¾ test sphere is limited. To avoid gaps between individual scans, 5 evenly separated by angle of 80gon setup points (P1, P2, P3, P5, P6) were chosen. In order to complete a polygon circle, a sixth position was introduced (P4), since no direct line of sight was possible between P3 and P5. The setup points are approximately 10m from the ¾ sphere.

In order to obtain measurements from the pole area of the ¾ sphere, a forklift truck was available. The MS50 could be placed in the forklift and an additional setup (E1) was made.

Figure 35 shows and overview of the measuring area with the different setup points.
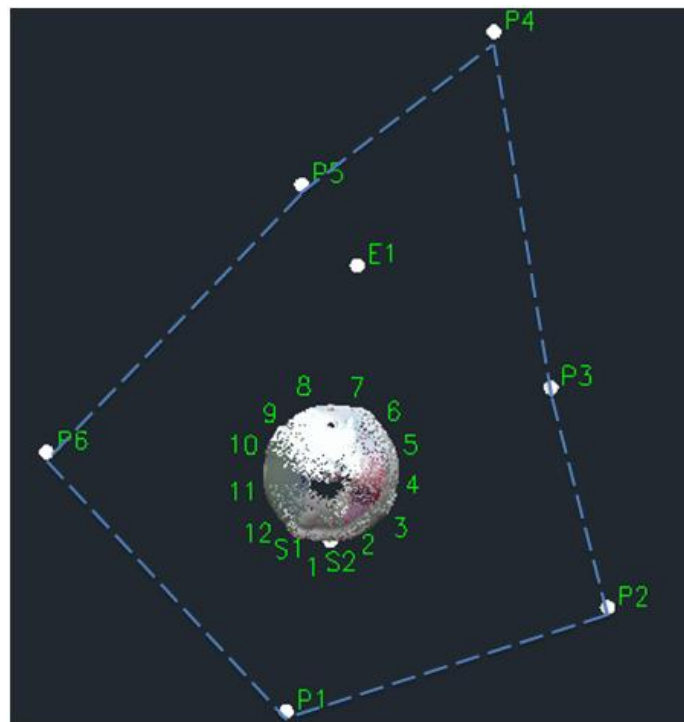
Figure 35: Measurement setup points

4.1.1 Local Coordinate System

The setup points were computed using the onboard software SmartWorx of the MS50 instrument. P1 was set as the starting point of the local coordinate system. The rotation of the local coordinate system was set to 0gon for the direction from P1 to S1, a bolt nut on the ¾ test sphere. Then a polygon circle was measured and the setup points P1 to P6 were marked on the ground. A transformation into another coordinate system was not necessary, since the purpose of these measurements is a comparison to a symmetric model.

4.1.2 Scan of the ¾ Sphere

After the coordinates of the setup points had been calculated, the scanning of the ¾ test sphere was the next step. Before every scan, the Leica MS50 was positioned on one of the setup points. By measuring the other visible setup points, the orientation cloud be calculated. After completing the setup, the scan area was defined measuring several points around the ¾ test sphere. To provide color information to the point cloud, the MS50 takes several images of the defined scan area, just before the scanning starts. All scans were carried out with the 1000 points per second option. This resulted in 7 individual scans, one from each of the setup points seen in Figure 35. P1 to P6 are setup points with known coordinates and ground markings, where the scan from P4 was used as redundancy. The setup point E1 was in the forklift truck, and the coordinates were derived by free stationing using measurements to P2, P5 and P6. Figure 36 shows the ¾ sphere as seen from the forklift (setup point E1).

Figure 36: View of the 3/4 sphere from the forklift (setup point E1)

Figure 37 shows a picture of the setup points P2 and P3 taken from the forklift.
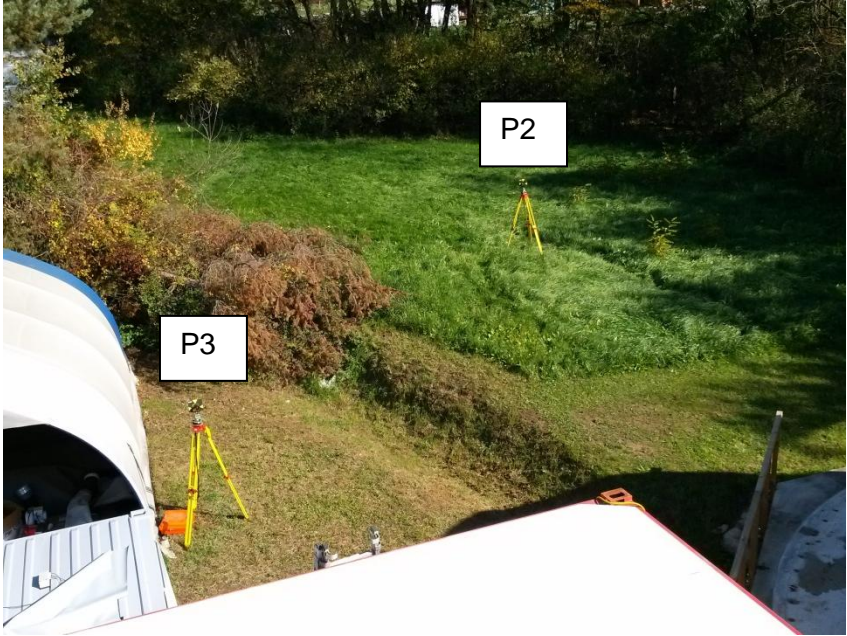

Figure 37: Setup points P2 and P3 as seen from the forklift truck

Figure 38 shows part of the ¾ sphere and the setup point P6 from the ground.
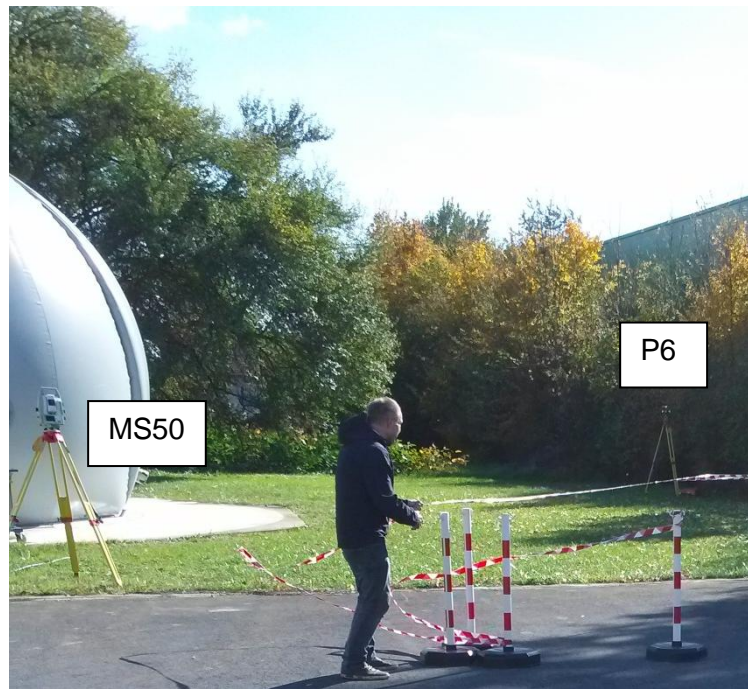
Figure 38: Setup point P6 and the 3/4 sphere

The resulting point cloud of the scan of the ¾ sphere can be seen in Figure 39, where the red lines show boundaries of individual scans.
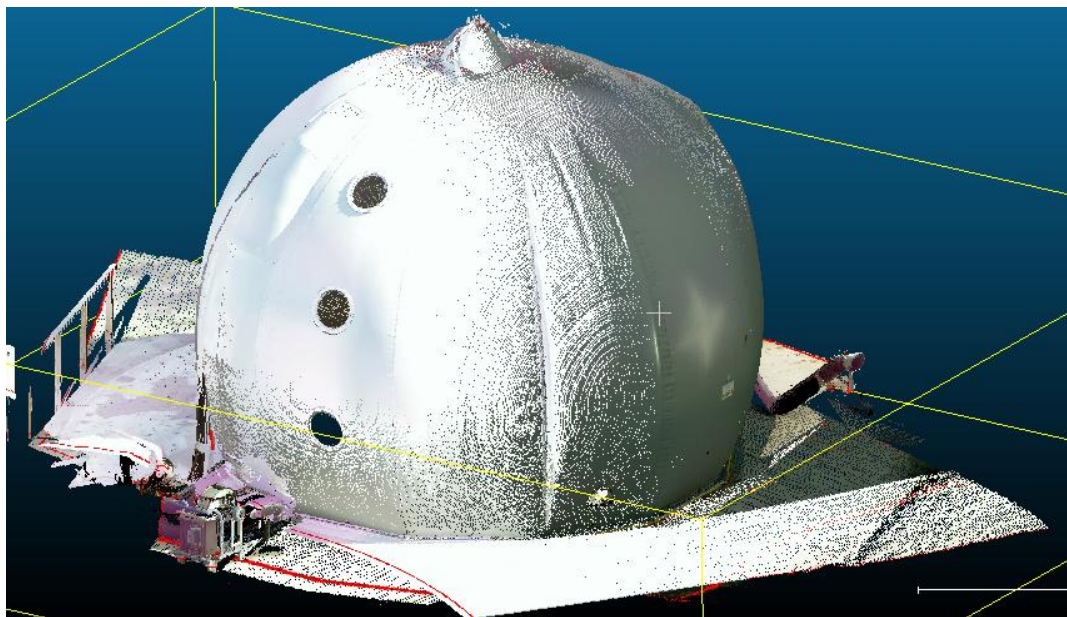

Figure 39: Scan of the ¾ sphere, fused from 7 individual scans

Since the forklift truck could not drive to the other side of the ¾ sphere, a small hole in the point cloud occurs as shown in Figure 40. It can also be seen that the point density decreases at the pole area.
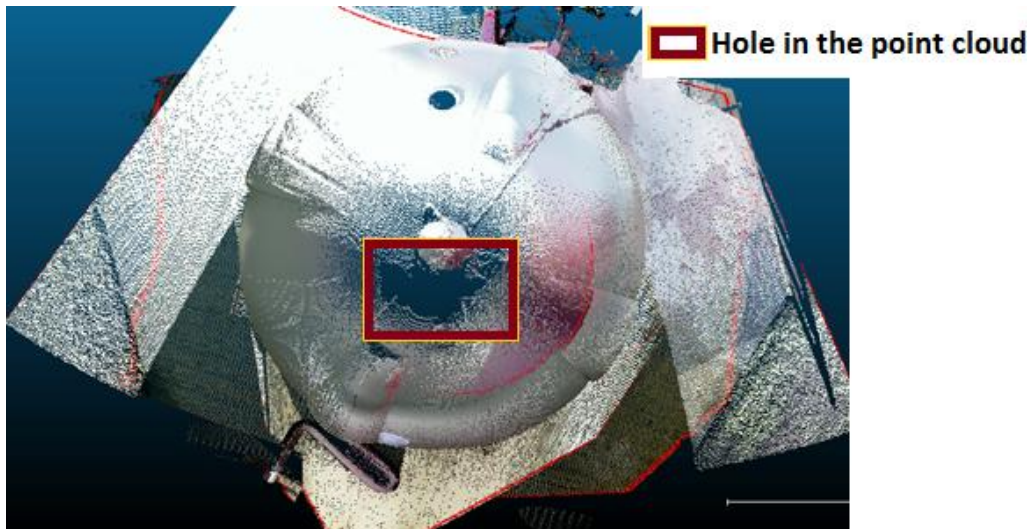
Figure 40: Hole in the point cloud due to inaccessibility

Additionally to the scans, some points of interest have been measured manually. These are the S1 nut bolt, the S2 (nut bolt at a window) and the 12 ground points. The ground points are at the connecting bolts of the membrane to the ground. These points of interest have been imported into AutoCAD and can be seen in Figure 41.
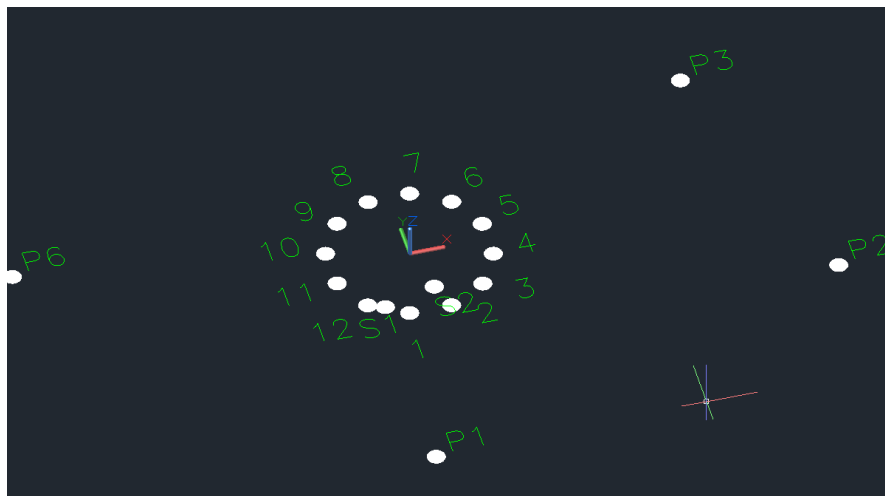

Figure 41: Points of interest, manually measured and shown in AutoCAD

The result from the field measurements is the 3D point cloud of the ¾ sphere with detail points.

5   Point Cloud Differences

This chapter looks into the acquired point cloud of the ¾ sphere. This point cloud represents the real geometry of the ¾ sphere. The model point cloud, provided by Sattler AG, represents the finite element model of the ¾ sphere. For better analysis of the shape difference between the model and the real geometry, point cloud differences have been computed. Additionally some sections of the point cloud analyzed in greater detail, to determine the behavior of the ¾ sphere along a welding seam and around the air-flow channels.

5.1   Software "CloudCompare"

To compute the point cloud differences, the open source software CloudCompare has been used. CloudCompare is freely available at danielgm.net/cc.

5.1.1   Preparing the Point Cloud

Before the differences of the point clouds can be computed, the surroundings must be cut out to isolate the ¾ sphere. This was done in CloudCompare (CC) with the segment tool and the result is shown in Figure 42.
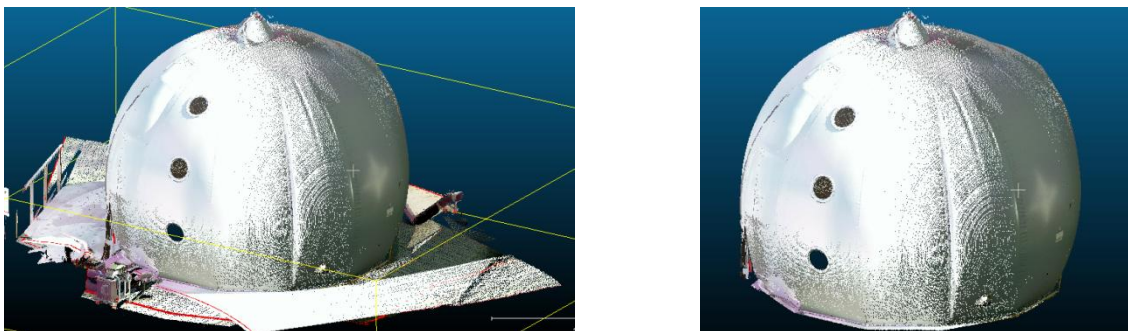

Figure 42: Segmentation of the 3/4 sphere point cloud, before (left) and after (right)

Now that the area of interest is separated, the point cloud has to be aligned to the reference model. Since the two point clouds are in different coordinate systems, equivalent points in both clouds have to be found. At the scanning of the ¾ sphere, the 12 ground points have been measured as well (chapter 4.1.2). These ground points are also visible in the reference model. Because the connection to the ground is basically a prerequisite, the scanned point cloud was aligned to the reference model using those ground points. CloudCompare then calculates a transformation matrix to align the scanned point cloud to the reference model using least squares adjustment. Figure 43 shows the alignment tool in CloudCompare and the resulting transformation matrix. The RMS (root mean square) of the transformation is 1.5cm. This deviation can be explained by an imperfect realization of the ground connection.
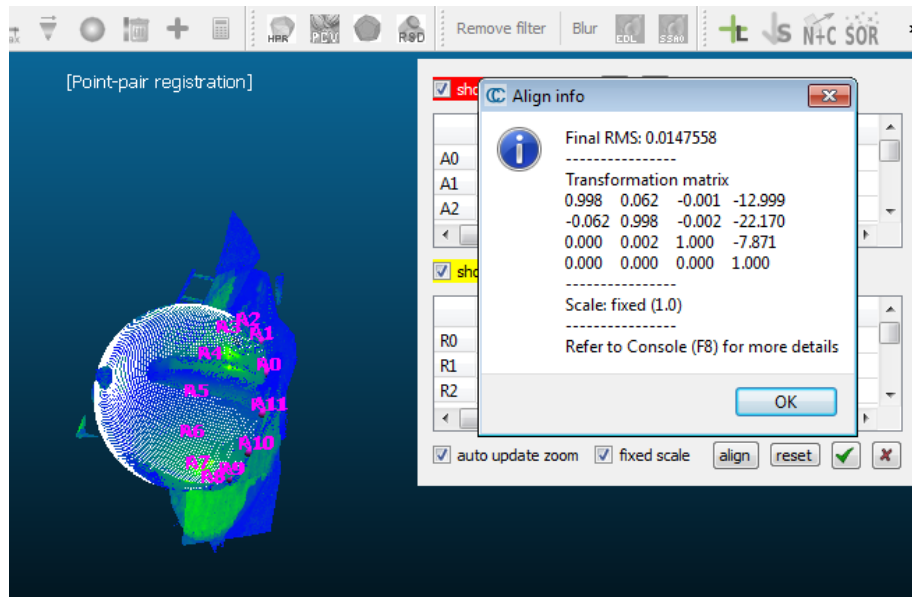
Figure 43: Alignment of the point cloud to the reference model in CloudCompare

5.1.2 Calculating the Point Cloud Difference

When comparing two point clouds, the simplest method would be a nearest neighbor search. This will work satisfactory when the reference cloud has sufficient density, since the calculated distance will slightly differ from the true distance as illustrated in Figure 44 left. CloudCompare offers a function in which local modeling can be applied, so the neighboring points of corresponding points are taken into account (Figure 44 right). This improves precision, but the software still only delivers absolute distances. This means it cannot be differentiated if the point lies inside or outside the reference model.
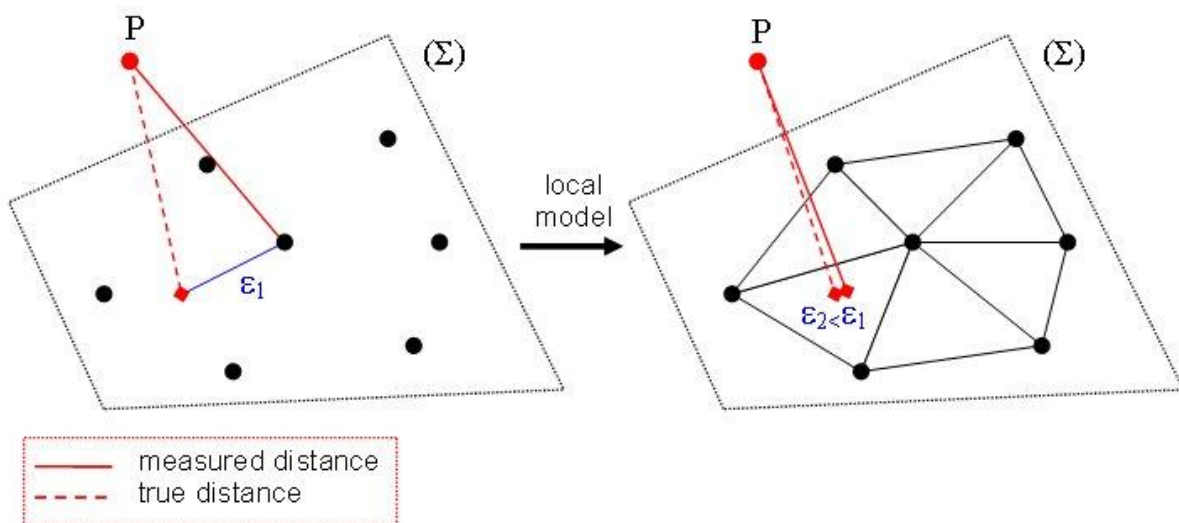

Figure 44: Illustration of cloud to cloud distance computation. The left image shows nearest neighbor detection, the right image the orthogonal distance to a triangulated local model (CC, 2012)

Since the reference model of the ¾ sphere does not provide sufficient density and signed distances are needed, the cloud to cloud compare approach does not meet the requirements. Therefore the reference model is loaded as a mesh (wireframe). The advantage of a mesh is that every face has a surface normal and therefore signed distances can be computed. CloudCompare also offers a function to calculate cloud to mesh distances. Figure 45 shows the reference mesh as loaded in CloudCompare.
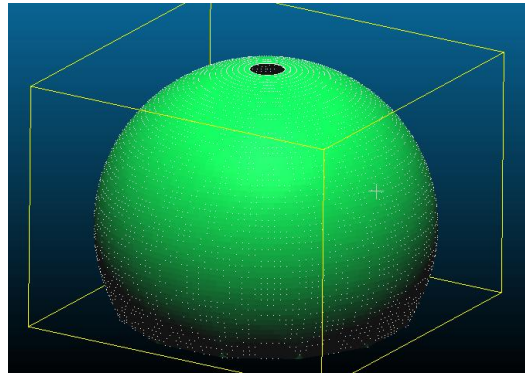

Figure 45: Mesh of the model point cloud

With the cloud to mesh distance function, the signed distance from every point to the reference mesh can be computed. The distances are then saved as a scalar field of the point cloud. The result of this is shown in Figure 46.
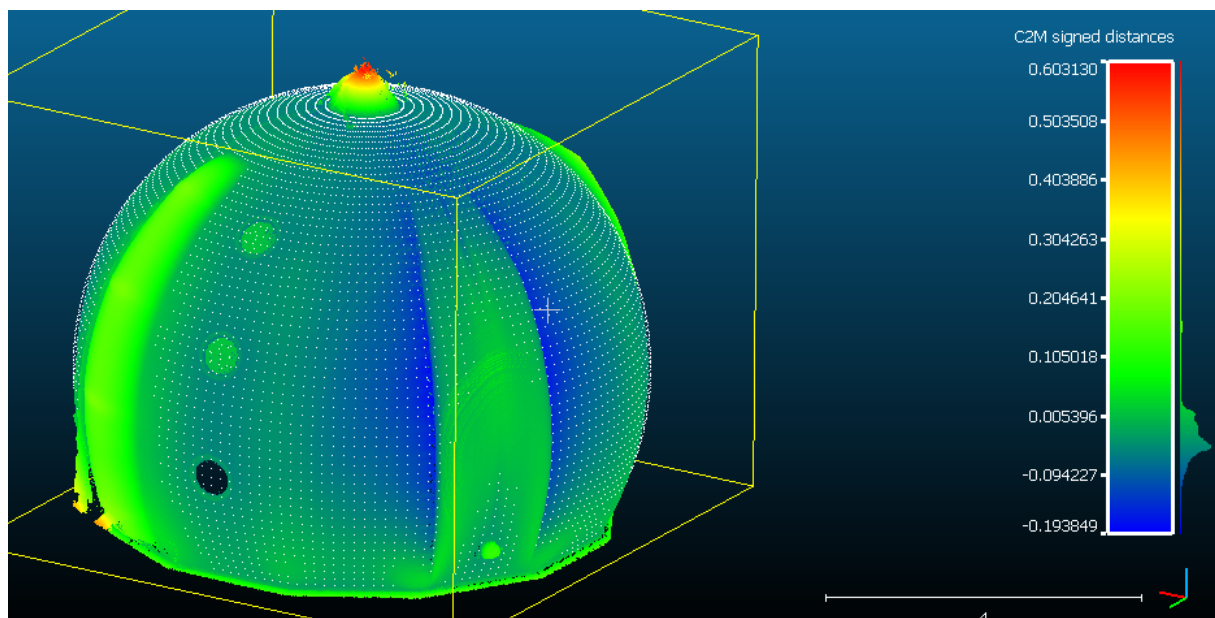
Figure 46: Point cloud differences to the reference mesh (unit of scale bar [m])

This point cloud can now be saved in ASCII format, which makes this point cloud very easy to import into other software. For further visualization, the software AutoCAD was chosen.
To be able to work with this point cloud in AutoCAD, the file format has to be rearranged, since AutoCAD does not support scalar fields in ASCII files. This was done with Matlab,

where for every point depending on the calculated distance a color in RGB was assigned. This leads to a color coded point cloud in AutoCAD as shown in Figure 47.
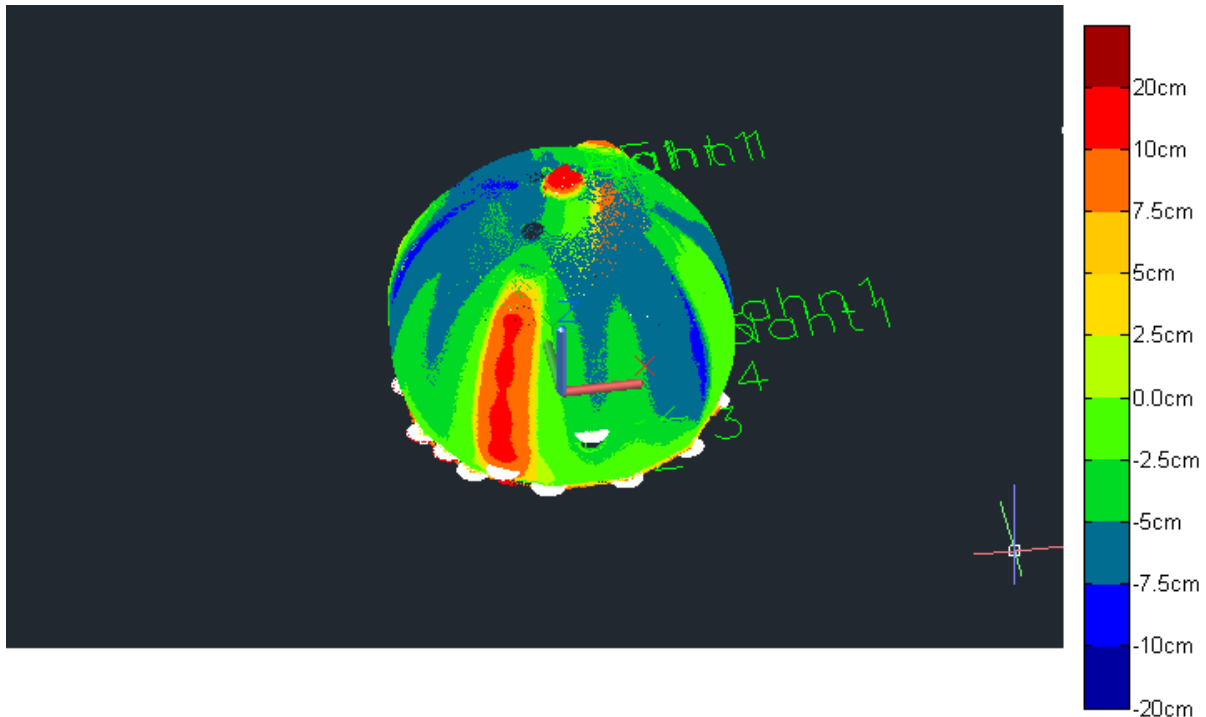

Figure 47: Point cloud differences in AutoCAD

At a first glance the air flow channels are prominent. This is because they are not part of the reference model. Also the deformations around the air flow channels as well as the welding seams can be seen.

The calculated point cloud differences are in respect to the reference model. To have a better understanding of the reference model, a perfect sphere was fitted into the reference model point cloud using least squares adjustment. The distance from every point of the reference model to that perfect sphere was calculated in Matlab and then visualized in CloudCompare. The result can be seen in Figure 48.
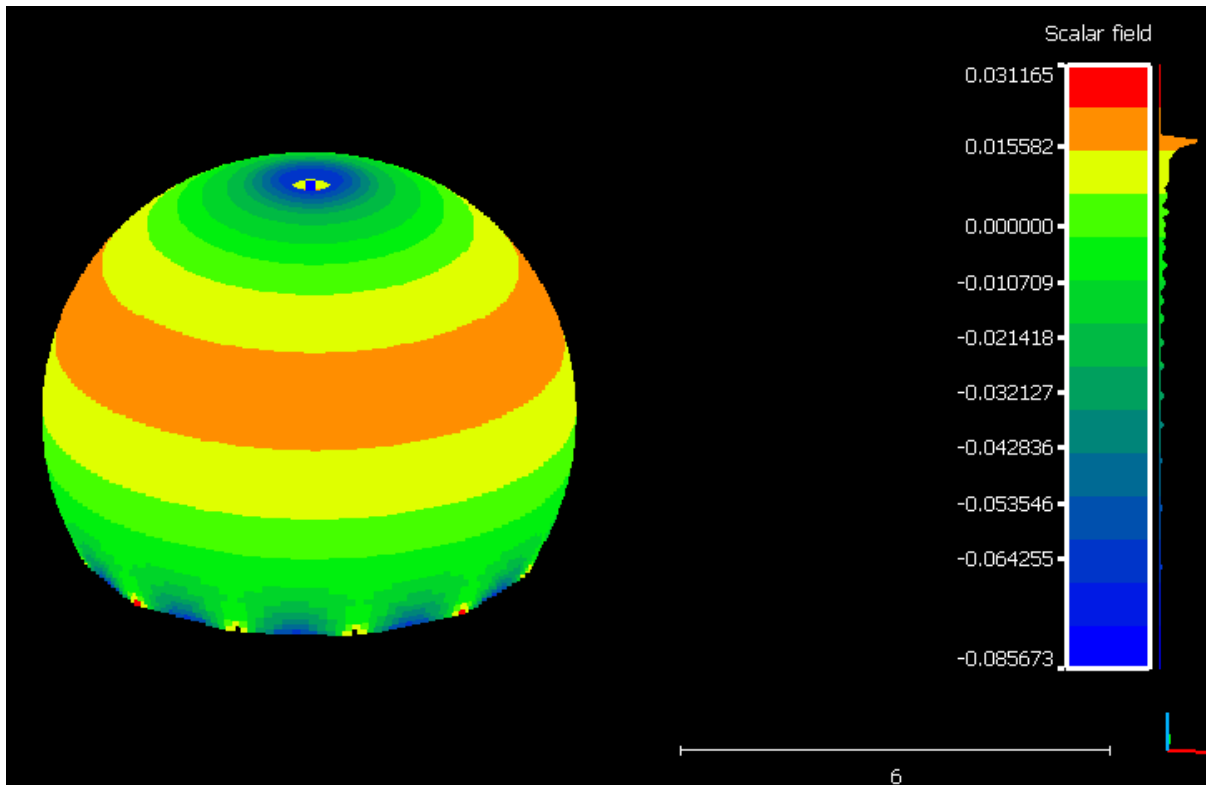
Figure 48: Reference point cloud differences to a perfect sphere which was fitted using least squares adjustment

It can be seen, that the reference model takes several parameters for deformations into account, such as the ground connection points and pole flattening.

5.2 Sections of Interest

The result from CloudCompare (ASCII PTS file) was imported into Matlab for further analysis of the point cloud differences. For this purpose, a Matlab program was developed, where section planes can be defined with three points. The distance to this plane is then calculated for every point of the point cloud and the reference model. Every point which is as close as 1cm to the section plane is then saved into the section cloud. Figure 49 shows an example for a section plane in AutoCAD, to visualize the concept that was implemented in Matlab.
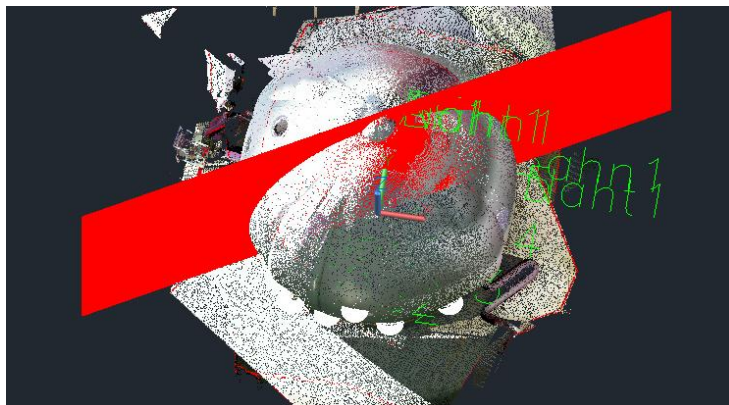

Figure 49: Visualization of an example section through the point cloud

With this concept, a variety of sections were sliced from the point cloud.

5.2.1 Visualization with Animated GIFs

To generate sequences of images, the ¾ sphere was sliced horizontally in approximately 10cm steps using the Matlab program described in chapter 5.2. The resulting section clouds were than saved as individual images in PNG format. These individual images were then sorted in Adobe Flash and exported as an animated GIF.

The ¾ sphere was also sliced vertically. Here the section plane was rotated in 6° steps and another animated GIF was generated. Figure 50 shows the starting picture for the GIFs, Figure 51 shows the sections in 4m height and 18° rotation.
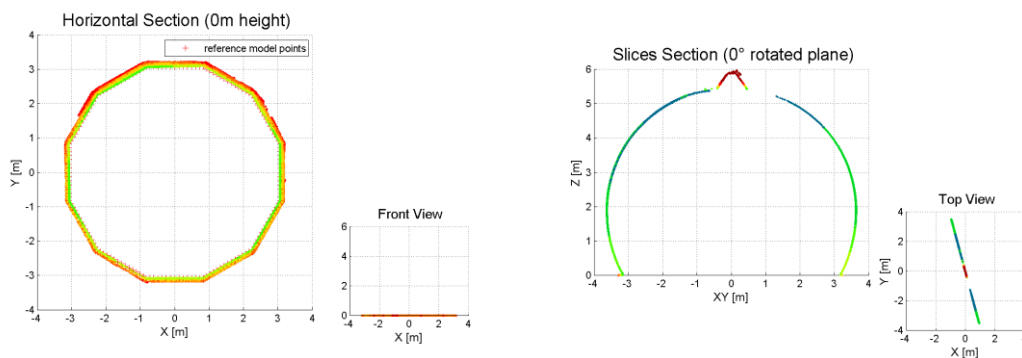
Figure 50: Starting picture for the generated GIFs, horizontal slices (left) and the vertical, rotated slices (right).
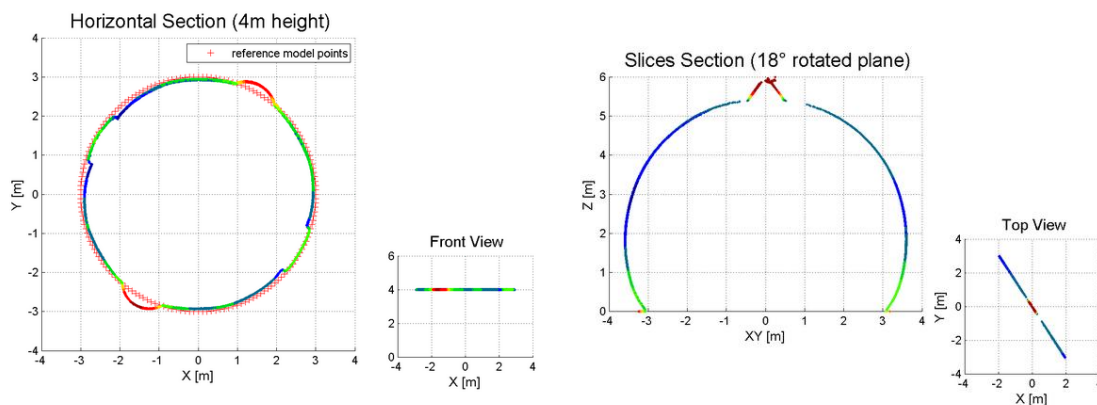
Figure 51: Horizontal section in 4m height (left) and vertical section with 18° rotated section plane (right)

5.2.2 Analysis of the Air Flow Channels

Figure 52 shows in which order the air flow channels are numbered and referred to in the following sections. Here the air flow channels 1 and 3 have similar design and the air flow channels 2 and 4 have similar design.

Figure 52: Overview of the 3/4 sphere and numbered air flow channels

In Figure 52 it can also be seen, that the air flow channel 1 creates ripples on the ¾ sphere. To analyze this further, a section next to this air flow channel was created. This section can be seen in Figure 53.
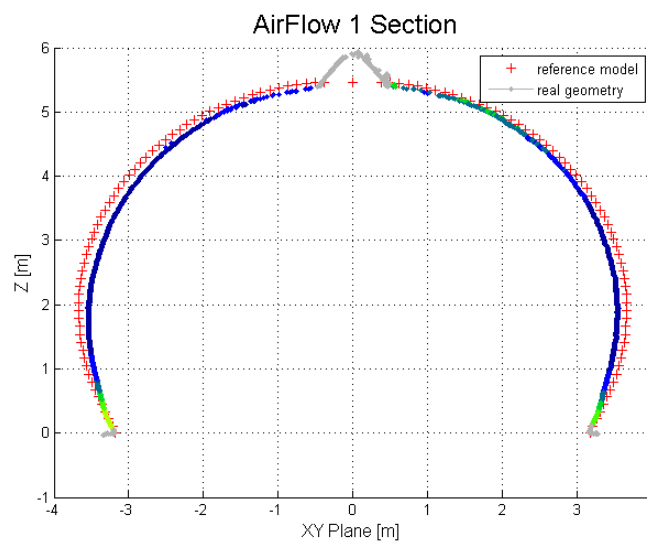

Figure 53: Section next to air flow channel 1 from the point cloud and the reference model

In Figure 53 the distances at the pole were colored gray, since the reference model does not account for the pole cap. To better see the differences from the real geometry to the reference model, another plot was generated. Here the distances are plotted along the profile, starting from one end of the section to the other. This can be seen in Figure 54.
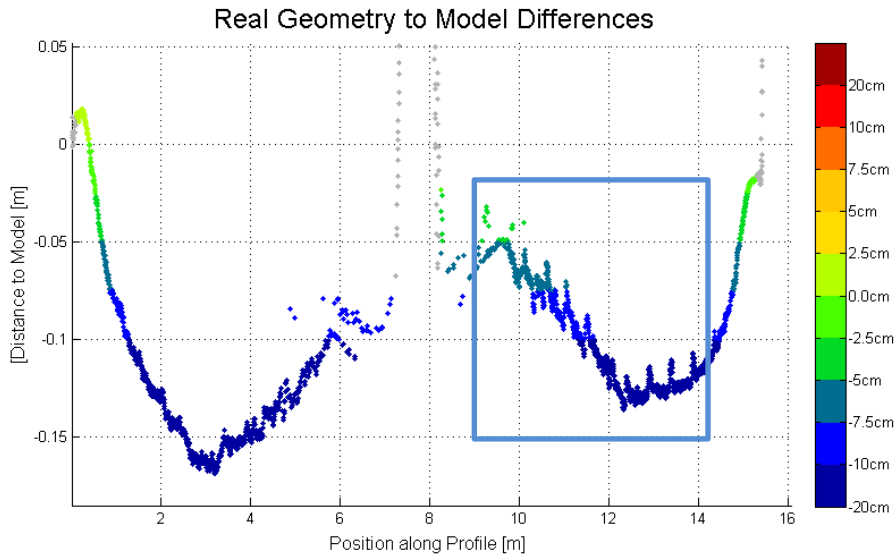
Figure 54: Differences along the section next to an air flow channel and the reference model. The blue rectangle marks the ripples, which are examined closer

In Figure 54 a long wave part can be seen, as well as the short wave ripples, which are marked by a rectangle. These ripples between the positions on the mesh 10m and 14m can also be seen in a close up in Figure 55.
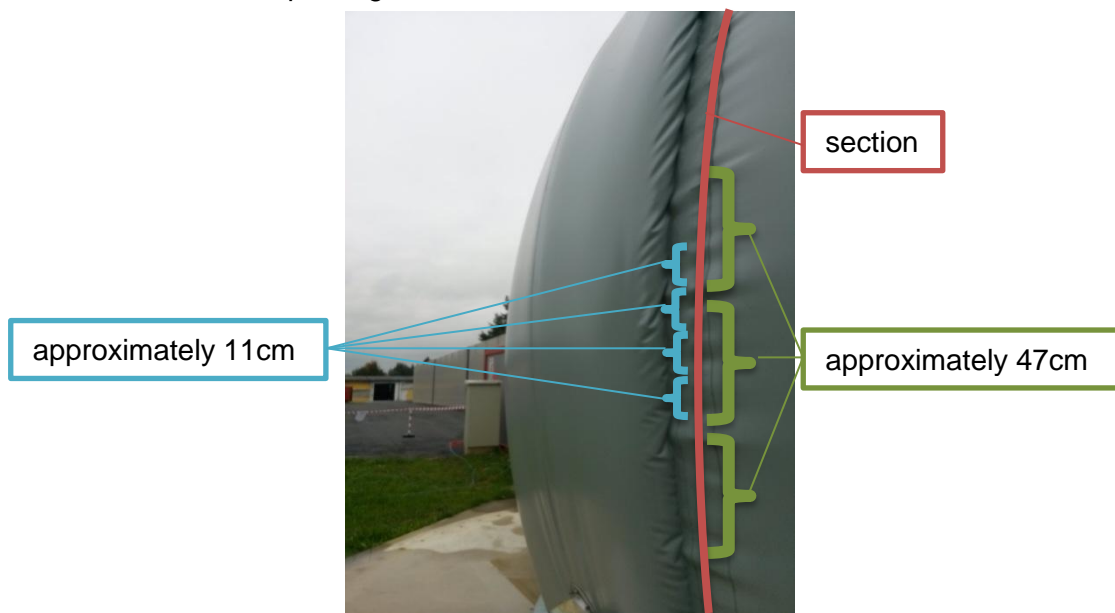
Figure 55: Deformations along an air flow channel, the section is visualized with a red line and the approximate ripple wave length is indicated in blue (11cm) and green (47cm)

For a closer look at the deformations, the long wave part was removed by subtracting a polynomial of degree 4. A Fourier transformation was applied to the corrected data. The resulting amplitudes are shown in Figure 56.
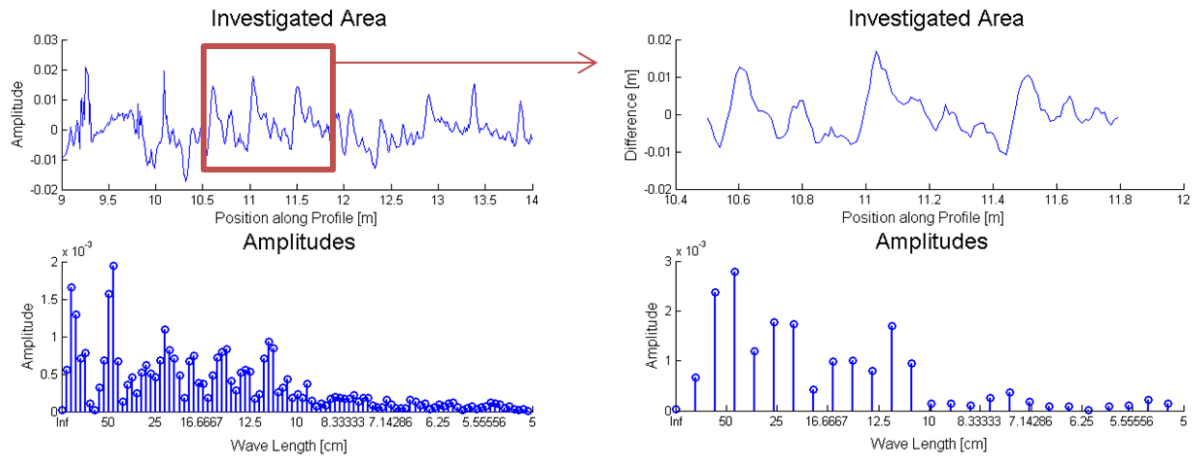
Figure 56: Fourier transformation of parts of the point cloud section next to air flow channel 1 (9m – 14m left, 10.5m – 11.8m right)

Table 17 shows the wave lengths that were calculated in the analysis of the section next to air flow channel 1. The Fourier transformation returns highest amplitudes at 47cm and 11cm.

Table 17: Detected deformation wave lengths of the section next to air flow channel 1

Fourier Transformation		
Wavelength	47cm	11cm

In general, the highest distances to the reference model are expected at the four air flow channels, since the reference model does not account for them. This leads to the case, that small distances to the reference model along the air flow channels mean that they cause high deformations. The similar designed air flow channels 1 and 3 can be seen in Figure 57, where the appealingly small distances show that these air flow channels cause deformations on the ¾ sphere. In Figure 58 the similar designed air flow channels 2 and 4 can be seen, where the expected higher distances to the reference model appear, which means that these designs have less of an impact on the shape of the ¾ sphere.
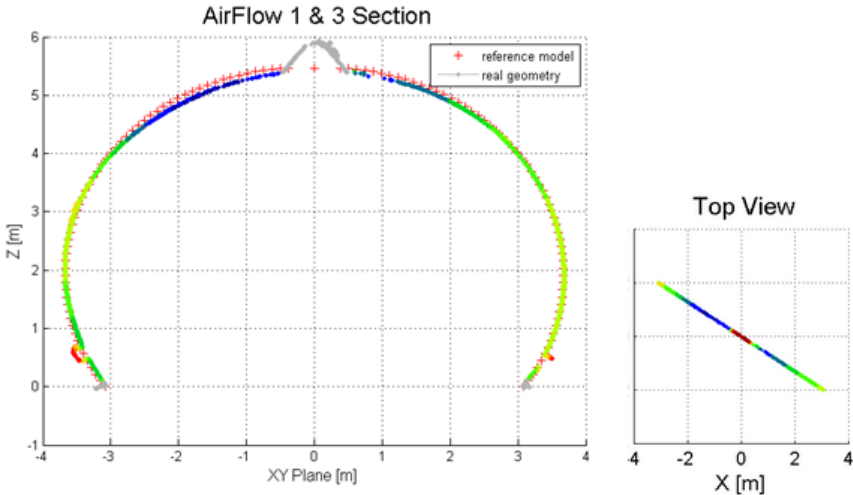
Figure 57: Section through air flow channel 1 (left half) and 3 (right half)
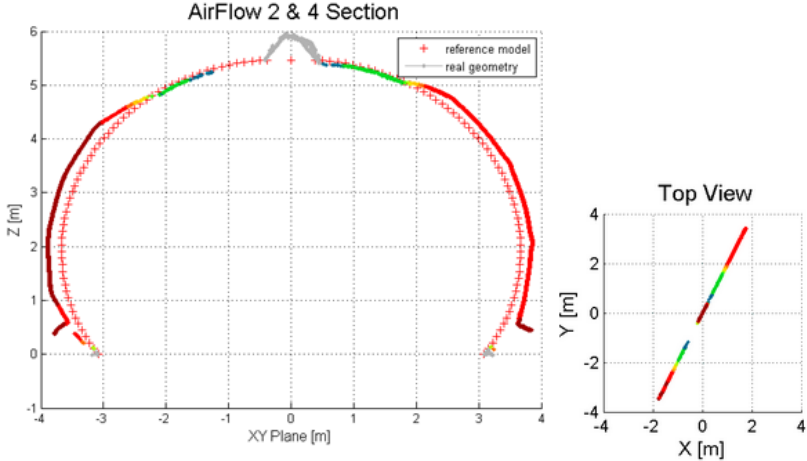

Figure 58: Section through air flow channel 2 (left half) and 4 (right half)

The deformation caused by the air flow channels can best be seen in the horizontal sections, as in Figure 51.

6   Results

The result of this thesis is a tested approach towards measuring 3D objects. The chain from research, testing, application and measuring, until analysis has been completed.

The workflow to determine the geometry, calculate the point cloud differences and visualize the results is shown in Figure 59. After measuring the object (scanning with the MS50), a 3D point cloud is created. The file format (SDB) hast to be converted to ASCII (PTS) with the software Infinity, to use the point cloud in other software. The point cloud can be aligned with a reference model (in DXF format) with the software CloudCompare, which also calculates the distances to the reference model for every point. This is again available in ASCII format and can be used in other software, such as AutoCAD or Matlab. In AutoCAD the manually measured connecting bolts are imported as blocks and the drawing can be saved as DWG. Further investigations with sections are performed in Matlab, where images are saved in PNG format. In Adobe Flash those images can be combined into animated GIFs, which can be viewed in Graphic Viewers, or any Web Browser.
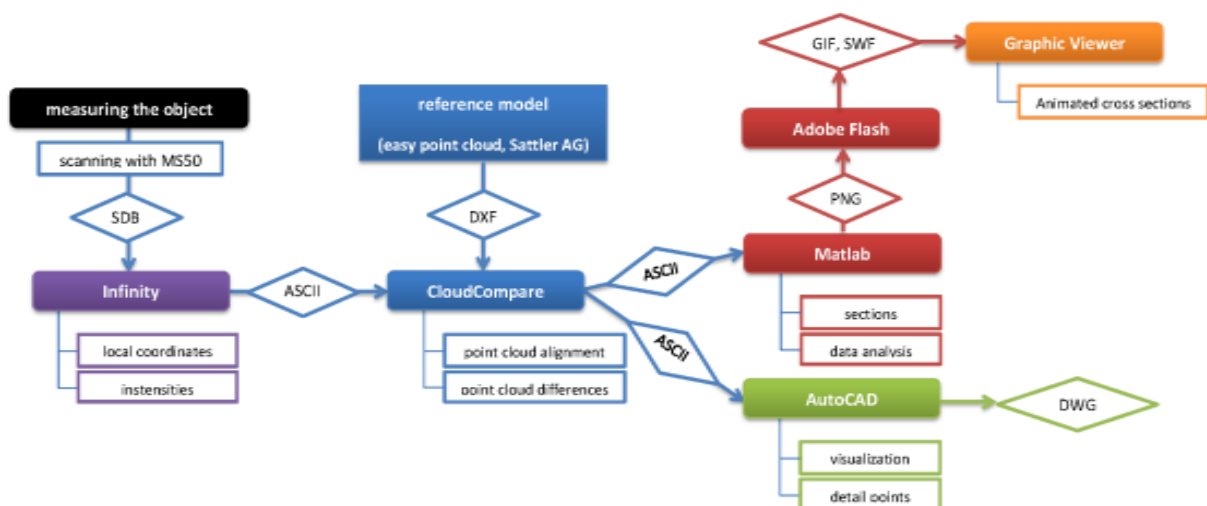

Figure 59: Schematic showing the workflow from measuring to visualization of the results

7 Conclusions and Discussion

To determine the geometry of biogas storage systems, different approaches have been explored. To measure the whole shape, a scanning total station was found to be the most suited for the given requirements. This recommendation was evaluated in the laboratory, by investigating the impact of the incident angle to the surface, the structure of the used material and the resolution of the scan function.

The next step was to measure a real test object – a ¾ sphere in Rudersdorf. A local coordinate system was easily realized with the total station and seven individual scans could be combined into one point cloud in the field.

For further analysis and visualization of the resulting point cloud, the point cloud was converted into ASCII (PTS) format, which can be used in almost any other software. The open source software CloudCompare was used, to generate the point cloud difference from the measured geometry to the reference model. With the results of CloudCompare, the deformations of the ¾ sphere could be visualized in AutoCAD. Especially the impact of the differently designed air flow channels on the geometry of the biogas storage system was prominent. To facilitate further analysis, sections were sliced from the point cloud, by developing software in Matlab. The resulting sections were saved as images (PNG) and combined into animated GIFs using Adobe Flash for better visualization.

A workflow to determine the geometry of biogas storage systems has been developed and tested. The whole process from data acquisition to data analysis and visualization was completed.

The ¾ sphere is now available as a 3D model and can be further analyzed using a variety of software, since it is available in ASCII format. The most prominent influence on the geometry of the ¾ sphere stems from the air flow channels. Since the test object has 4 different air flow channels, their influence on the geometry can be taken into account when choosing one design. Additionally the ¾ sphere was sliced into many sections and is available in animated GIFs.

The results of this thesis show the high flexibility and the wide area of application for modern total stations. Especially for objects with more complex geometry the scan function offers a quick solution to a complex problem. Also the ability to set up a local coordinate system containing all taken measurements is a big advantage of this system. The measurement plan can be adjusted according to real-time views of the already measured data. This way mistakes can be avoided and additional points of interest easily implemented.

The knowledge of the real geometry of biogas storage systems can help choosing different designs, for example of the air flow channels. By decreasing the deformations, the stress on the welding seams can also be decreased and thus damages can be avoided. For this thesis, only one test object of a biogas storage system was measured, but with the efficient workflow provided, the geometry of different designs and sizes of biogas storage systems could also be measured, which could lead to a more efficient manufacturing process.

References

ABB (2013) Analytical Measurements Level Products Brochure – Level Measurement using Laser Technology, Level and volume measurement solutions for process and utility application

ABER JS, MARZOLF I, RIES JB (2010) Small-Format Aerial Photography: Principles, Techniques and Applications, Elsevier B.V., 32-33

BADER K (2001) Presentation – Photometrische Stereoanalyse, Hauptseminar Computer Vision, Kapitel VIII

CC (2012) CloudCompare Wiki - http://www.danielgm.net/cc/doc/wiki (last visit: 01.05.2014)

DIRECTINDUSTRY (2013) http://www.directindustry.de/industrie-hersteller/koordinatenmessmaschine-72392.html (last visit: 01.05.2014)

EEX (2013) Brochure – At the Centre of European Energy Trading, 29

FARO (2013) http://www.faro.com/products/metrology/faro-laser-tracker/overview (last visit: 01.05.2013)

FSG (2013) http://www.fernsteuergeraete.de/de/produkte/seilzuggeber.html (last visit: 12.12.2013)

GE (2010) Brochure – GE Measurement & Control Solutions, X-ray inspection, computed tomography and 3D metrology

GISBOX (2013) http://www.gisbox.ro/index.php?p=22 (last visit: 01.05.2014)

GOM (2013) http://www.gom.com/metrology-systems/3d-scanner.html (last visit: 01.05.2014)

HANDSCHUH C (2009) Einsatz von Normalmaps in der Postproduktion, GRIN Verlag, 33-34

HEXAGON (2008) White Paper – The Leica Absolute Interferometer, A New Approach to Laser Tracker Absolute Distance Meters

KAMMEL S (2004) Deflektometrische Untersuchung spiegelnd reflektierender Freiformflächen, Schriftenreihe Institut für Mess – und Regelungstechnik, Universität Karlsruhe Nr. 004, 10-13

KRICH K, AUGENSEIN D, BATMALE JP, BENEMANN J, RUTLEDGE B, SALOUR D (2005) Biomethane from Dairy Waste. A Sourcebook for the Production and Use of Renewable Natural Gas in California, 71-76

LEICA (2013a) Brochure – Leica Nova MS50

LEICA (2013b) Datasheet – Leica Nova MS50

LINDSTAED M, GRAEGER T, MECHELKE K, KERSTEN T (2011) Terrestrische Laserscanner im Prüfstand – Geometrische Genauigkeitsuntersuchungen aktueller terrestrischer Laserscanner

LÖFFLER F (2002) Maschinen – und Anlagenbau, 2. Auflage, 147-275

MAZAHERI M, MOMENI M (2008) 3D Modeling Using Structured Light Pattern and Photogrammetric Epipolar Geometry. Dept of Geomatic Engineering University of Isfahan

SALUNKHE, D B (2012) Biogas Technology. International journal of engineering science and technology Vol. 4. 1-2

SATTLER AG (2010) Internal Report – Prüfbericht Vermessung Biogasanlage. Sigma3D GmbH, 1-18

SATTLER AG (2012) Brochure – Biogas Storage Systems. Environment Engineering, 1-16

SCHENK T (2005) Introduction to Photogrammetry, Department of Civil and Environmental Engineering and Geodetic Science, The Ohio State University, 49-61

SCHWARZENBERG GF (2008) Untersuchung der Abbildungseigenschaften eines 3D-Ultraschall-Computertomographen zur Berechnung der 3D-Abbildungsfunktion und Herleitung einer optimierten Sensorgeometrie. Karlsruhe Series on Intelligent Sensor-Actuator-Systems. XIII

SMITH C (2009) Basic Process Measurements. John Wiley & Sons Inc., Hoboken, New Jersey.

STATISTA (2014) http://de.statista.com/statistik/daten/studie/167671/umfrage/anzahl-der-biogasanlagen-in-deutschland-seit-1992/ (last visit: 12.12.2013)

TRAGNER F (2008) Biogas-Branchenmonitor. Erhebung von Wirtschaftsdaten und Trends zu Biogas in Österreich, Bundesministerium für Verkehr, Innovation und Technologie, 4-8

Zoller + Fröhlich (2013) Brochure – ZF Imager 5010. 01/2013